Lipid perturbation compromises UPR-mediated ER homeostasis as a result of premature degradation of membrane proteins

Benjamin S.H. Ng[1], Peter Jr. Shyu[1], Ruijie Chaw[1], Seah Yi Ling[1], Guillaume Thibault[1,2]

[1]School of Biological Sciences, Nanyang Technological University, Singapore, 637551
[2]Lee Kong Chian School of Medicine, Nanyang Technological University, Singapore, 308232

Character count: 45,892 (no spaces)

Correspondence to:

Guillaume Thibault, Tel: +65 6592 1787; Fax: +65 6791 3856; email: thibault@ntu.edu.sg

Running title: Lipid perturbation destabilises a subset of transmembrane proteins

ABSTRACT

Phospholipid homeostasis in biological membranes is essential to maintain cellular functions of organelles such as the endoplasmic reticulum. Phospholipid perturbation has been associated to non-alcoholic fatty liver disease, obesity and other metabolic disorders. However, in most cases, the biological significance of lipid disequilibrium remains unclear. Previously, we reported that *Saccharomyces cerevisiae* adapts to lipid disequilibrium by upregulating several protein quality control pathways such as the endoplasmic reticulum-associated degradation (ERAD) pathway and the unfolded protein response. Surprisingly, we observed certain ER-resident transmembrane proteins (TPs), part of the UPR programme, to be destabilised under lipid perturbation (LP). Among these, Sbh1 was prematurely degraded by dissociating from the Sec61 complex due to fatty acid remodelling and membrane stiffening of the ER. Sbh1 is targeted for degradation through its highly conserved lysine residue near the membrane in a Doa10-dependent manner. Premature removal of key ER-resident TPs might be an underlying cause of chronic ER stress in metabolic disorders.

INTRODUCTION

Phospholipid homeostasis is crucial in the maintenance of various cellular processes and functions. They participate extensively in the formation of biological membranes, which serve to generate distinct intracellular environments into ordered infrastructures known as organelles for metabolic reactions, storage of materials, signalling, as well as sequestration of metabolites. Existing in various distinct molecular species, phospholipids are regulated within relatively narrow limits and their composition in biological membranes among organelles differs significantly (van Meer, Voelker, & Feigenson, 2008).

It is widely established that the perturbation of the two most abundant phospholipids, phosphatidylcholine (PC) and phosphatidylethanolamine (PE) levels can lead to various disease outcomes such as non-alcoholic fatty liver disease (NAFLD) (Arendt et al., 2013; Buang, Wang, Cha, Nagao, & Yanagita, 2005; Corbin & Zeisel, 2012; Li et al., 2006), type II diabetes (T2D) (Kim et al., 2016), as well as cardiac and muscular dystrophies (Mitsuhashi & Nishino, 2011). Being highly abundant in the biological membranes of organelles such as the endoplasmic reticulum (ER), the perturbation of PC and PE levels results in ER stress (D. E. Vance, 2014). For instance, an elevated PC/PE ratio in obesity was found to contribute to the development of NAFLD (Fu et al., 2011; Jacobs et al., 2010). Perturbation in phospholipids was shown to cause the premature degradation of the sarco/endoplasmic reticulum Ca^{2+}-ATPase (SERCA) ion pump, disrupting calcium homeostasis and resulting in chronic ER stress. This eventually resulted in hepatic steatosis and liver failure. In another study, mice fed with high fat diet exhibited an increase in gut microbiota enzymatic activity that have been shown to lead to reduced choline (Dumas et al., 2006; Nicholson et al., 2012). Choline is an essential dietary nutrient primarily metabolised in the liver and used for the synthesis of PC. Similarly, choline deficiency may play an active role in the development of insulin resistance. However, the molecular events leading to the development of chronic ER stress and metabolic diseases such as NAFLD from lipid perturbation (LP) remains largely unknown.

In *Saccharomyces cerevisiae*, *de novo* synthesis of PC is catalysed by the enzymes Cho2 and Opi3, while carried out by the homolog of Opi3, PEMT, in mammals (Figure 1A). Cho2 firstly methylates PE to N-monomethyl phosphatidylethanolamine (MMPE), which is then further methylated by Opi3 to PC through the intermediate N, N-dimethyl phosphatidyl-ethanolamine (DMPE). Alternatively, PC is

synthesised from choline, when available, through the Kennedy pathway. Both pathways are highly conserved from yeast to humans. It has been reported that *PEMT*$^{-/-}$ mice develop NAFLD within three days of choline deficient diet (Li et al., 2006). Previously, we developed a LP model to mimic NAFLD by deleting the gene *OPI3* (Thibault et al., 2012).

The unfolded protein response (UPR) is a stress response pathway monitoring ER stress to restore cellular homeostasis (Cox, Shamu, & Walter, 1993). Upon accumulation of misfolded proteins, the UPR is activated and alleviates stress by reversing severe dysfunctions through the upregulation of nearly 400 target genes in yeast (Travers et al., 2000). Major targeted regulatory pathways includes cytosolic protein quality control (CytoQC), ER-associated degradation (ERAD), protein translocation, protein modification and phospholipid biosynthesis (Thibault, Ismail, & Ng, 2011; Travers et al., 2000). By increasing ER protein folding capacity and enhanced clearance of misfolded proteins coupled with a general attenuation of protein translation (Harding, Zhang, & Ron, 1999), the UPR strives to achieve ER homeostasis.

Recently, it was demonstrated that the UPR is essential in alleviating ER stress in lipid dysregulated cells to maintain protein biogenesis, protein quality control and membrane integrity (Costanzo et al., 2010; Schuldiner et al., 2005; Thibault et al., 2012; Volmer & Ron, 2015). LP from the absence of *CHO2* or *OPI3* exhibits synthetic lethality with the only UPR signalling transducer in yeast, *IRE1*, as well as its downstream transcription factor *HAC1* (Costanzo et al., 2010; Schuldiner et al., 2005). LP has been well characterised to induce ER stress (Jonikas et al., 2009; Promlek et al., 2011; Volmer, van der Ploeg, & Ron, 2013) and the failure of the UPR to restore homeostasis is implicated in several human diseases (Pagliassotti, 2012; Wu, Ng, & Thibault, 2014; Yang, Zhao, Ren, & Yang, 2015). This clearly establishes the critical role of the UPR in buffering the lethal effects of LP to ensure cell survival.

As altered PC levels are associated with obesity (Puri et al., 2007) and PC/PE imbalance has similarly been implicated in murine models of metabolic diseases (Fu et al., 2011), our previous work focused on the cellular stress response to PC/PE imbalance in yeast. We showed that altering PC metabolism in *S. cerevisiae* leads to predominant reprogramming of the protein homeostasis network (Thibault et al., 2012), thereby revealing previously unappreciated links between cellular lipid balance and protein

homeostasis. In this study, we observed certain ER-resident TPs, part of the UPR programme, to be prematurely degraded under LP. On one facet, we demonstrated that LP affects the ER membrane which results in the destabilisation of the TPs. On another facet, we elucidated the mechanism of how one of the prematurely degraded TPs, Sbh1, gets recognised for degradation through ERAD. Our findings reveal that under LP, TPs activated by the UPR programme are prematurely degraded due to changes in the membrane properties. They seem to be recognised and rapidly degraded by the exposure of certain degradation motif which became unembedded under LP.

RESULTS

A subset of transmembrane proteins is destabilised during lipid perturbation

Global transcriptional and proteomic analyses point out to a dramatically-altered biochemical landscape in yeast cells under lipid perturbation (LP) (Thibault et al., Mol Cell 2012). From that global analysis, we identified 66 proteins that were transcriptionally upregulated from the DNA microarray analyses, yet displayed a decrease in protein abundance from spectrometric protein analyses (Table S1). The list includes 11 ER-resident transmembrane proteins (TPs). To eliminate cellular functions affected from LP such as transport and secretion, we focused on ER-resident proteins. To confirm our previously published large-scale data, we analysed the steady-state level of ten TPs candidates under LP using PC synthesis deficient strain *opi3*Δ (Fig. 1A-B) (Thibault et al., Mol Cell 2012). Coy1, Cue1 and Erp5 were found to have similar protein steady-states in *opi3*Δ as compared to WT, while Ctr1, Nsg2, Sbh1 and Scs7 had significantly lower steady-state levels. Surprisingly, Emc4, Prm5 and Yet3 exhibited higher protein steady-states. Overall, the steady-state level of the TPs analysed is lower during LP suggesting that they are downregulated at the translational levels or that they are prematurely degraded.

Among these TPs, Cue1, Emc4, Nsg2, and Sbh1 were identified among the candidates as part of the UPR programme with Nsg2 and Sbh1 exhibiting a drastic decrease in protein abundance. Cue1 is an essential component of the ERAD pathway (Biederer, Volkwein, & Sommer, 1997). Emc4 is a member of the conserved ER transmembrane complex (EMC) and is required for efficient folding of proteins in the ER (Jonikas et al., 2009). EMC is also proposed to facilitate the transfer of phosphatidylserine from ER to mitochondria (Lahiri et al., 2014). Nsg2 regulates sterol-sensing protein Hmg2 (Flury et al., 2005).

The β subunit of Sec61 ER translocation complex, Sbh1, is highly conserved in eukaryotes and plays a role in the translocation of proteins into the ER (Fig. S1). It is non-essential for translocation but can cause a translocation defect when both Sbh1 and its homolog, Sbh2, are absent (Feng et al., 2007).

To assess the stability of TP candidates during lipid imbalance, cycloheximide chase assay was performed in WT and *opi3*Δ strains. Time points were taken from adding translation inhibitor cycloheximide to measure the half-life of HA tagged-proteins over a period of one hour. Emc4, Nsg2, and Sbh1 half-life were found to be significantly reduced under lipid disequilibrium (Fig. 1 C). No significant decrease in Cue1-HA protein level was detected in *opi3*Δ (*P* value of 0.051). After one hour chase, protein levels of Emc4, Nsg2, and Sbh1 were found to be 27%, 41%, and 58% lower in *opi3*Δ, respectively, compared to WT. This suggests that the UPR programme transcriptionally upregulates genes to restore ER homeostasis upon LP while a subset of TPs is degraded prematurely.

A subset of ER-localised transmembrane proteins is destabilised by a decrease in phosphatidylcholine

To ensure that Cue1, Emc4, Nsg2, and Sbh1 are not prematurely degraded due to mislocalisation, indirect immunofluorescence was performed with the four protein candidates. They were found to co-localise with the molecular chaperone ER marker Kar2 in *opi3*Δ as in WT (Fig. 2 A). To further confirm the four TPs remain inserted into the ER membrane, cell extracts from WT and *opi3*Δ strains expressing the four candidates were treated with alkali to strip soluble and peripherally associated protein from membranes (Stukey, McDonough, & Martin, 1989). Membranes and alkali-extracted proteins were separated by high speed centrifugation and detected by immunoblots. The four candidates were fractionated exclusively within the membrane pellet (Fig. 2 B). Together, these results suggest that localisation and integration of the four TPs into the ER membrane were unaffected by phosphatidylcholine depletion. To ensure the premature degradation of these four proteins is not due to inverted topology, we performed proteinase K (PK) digestion from isolated microsomes (Fig. 2 C). In WT cells, C-termini HA tags of Cue1-HA, Emc4-HA and Nsg2-HA are found in the cytosol. Thus, HA tag will be cleaved off if the topology is intact while a peptide will be detected if the topology is inverted upon PK digestion. The three proteins were found to be fully digested under LP and the predicted smaller protein fragments of 23.7, 8.53, and 5.8 kDa were not detected for Cue1-HA, Emc4-HA, and

Nsg2-HA, respectively, in both WT and *opi3*Δ. Sbh1-HA is a tail-anchored protein where the C-termini HA tag is found in the ER lumen, hence the predicted protein fragment of 10.5 kDa was detected in both WT and *opi3*Δ strains. Typically, tail-anchored proteins are tagged at the N-termini as C-termini interact with the Get complex for insertion into the ER membrane (F. Wang, Whynot, Tung, & Denic, 2011). Thus, this result combined with alkaline carbonate extraction show that adding a C-terminus HA tag to Sbh1 did not interfere with its integration into the ER membrane. Together, these results suggest that the four TP topologies are not affected from LP and thus eliminating this factor as an underlying cause for their premature degradation.

To further confirm the four candidate proteins are destabilised from low PC levels, their degradation was monitored in the presence of choline. Choline is rapidly converted into PC through the Kennedy pathway to restore PC level of *opi3*Δ similar to WT (Fig. 1 A) (Carman & Henry, 1989; Thibault et al., 2012). Choline supplementation in *opi3*Δ was sufficient to fully stabilise Cue1-HA, Emc4-HA, Nsg2-HA, and Sbh1-HA to the level found in WT (Fig. 2 D). Subsequently, we concentrated our effort on Sbh1 to better understand how a membrane protein is destabilised from LP.

The UPR is strongly activated in response to LP (Jonikas et al., 2009; Thibault et al., 2012). In *opi3*Δ, it can be referred as chronic ER stress as the constitutive UPR activation is strong (Thibault et al., 2012; Vevea et al., 2015). To ensure that Sbh1 is not destabilised from a strong UPR activation, we introduced a constitutive active form of the downstream effector, Hac1^{i}, into WT cells (Chapman & Walter, 1997; Thibault et al., 2011). As expected, constitutively activated UPR did not further destabilise Sbh1 in WT cells (Fig. S2). Noticeably, Sbh1 steady state is higher in UPR-activated WT cells as *SBH1* is upregulated from the UPR programme (Thibault et al., 2012; Travers et al., 2000). Thus, this indicates that the UPR activation in *opi3*Δ is not a contributor to Sbh1 premature degradation.

Changes in ER membrane fluidity is sufficient to destabilise Sbh1

To characterise lipid remodelling specific to the ER in *opi3*Δ that might contribute to the premature degradation of TPs, we analysed the fatty acid (FA) composition of whole cells and fractionated microsomes from WT and *opi3*Δ. Overall, total FAs in *opi3*Δ cells increased by 96% when compared to WT (Fig. 3 B). This was expected as *opi3*Δ accumulates large lipid droplets (Fei et al., 2011; Thibault

et al., 2012). From isolated microsomes, a large increase of the short FAs myristic acid (C14:0) and myristoleic acid (C14:1) and a decrease of oleic acid (C18:1) were observed in *opi3*Δ when compared to WT (Fig. 3 B, Fig. S3). Interestingly, lipid remodelling by the shortening of FA chains and increase in saturated FAs is more drastic in *opi3*Δ microsomes compared to whole cells (Fig. 3 B). In addition of FAs remodelling, the intermediate for the synthesis of PC from PE, MMPE, becomes the most abundant phospholipid with the depletion of *OPI3* as previously reported (Fig. 1 A) (Thibault et al., 2012). As MMPE is modified from PE by the addition of one methyl group, a large increase is expected to induce negative membrane curvature stress as previously reported for PE (J. E. Vance & Tasseva, 2013). The remodelling of FAs saturation state might be another adaptive response to alleviate membrane curvature stress in *opi3*Δ (Fig. 3 C) (Boumann et al., 2006; Zimmerberg & Kozlov, 2006). FA saturation states of biological membranes are highly linked to membrane fluidity (Quinn, 1981; Stubbs, 1983; Stubbs & Smith, 1984).

To better understand the impact of membrane remodelling on TPs mobility, we monitored the dynamic of the ER-resident membrane protein Sec63-GFP by fluorescent recovery after photobleaching (FRAP) (Shibata et al., 2008). A region of the cortical ER is photobleached and its fluorescent recovery is quantified which correlates with Sec63-GFP mobility. The fluorescent recovery of Sec63-GFP was significantly slower in *opi3*Δ compared to WT suggesting the ER membrane might be stiffer (Fig. 3 D, E, Fig. S4). This result is consistent with the reported observation that decreased PC/PE ratio stiffen the membranes (Boumann et al., 2006; Dawaliby et al., 2016). Taken together, it suggests that a decrease in membrane fluidity might cause the destabilisation of the TPs.

To further investigate the role of membrane fluidity on the stability of Sbh1, we introduced the stearoyl-CoA desaturase gene *OLE1* under the control of the expression promoter *PRC1* to increase monounsaturated fatty acids (MUFAs) over saturated fatty acids to elevate membrane fluidity (Snider, Kittanakom, Curak, & Stagljar, 2010). As *OLE1* is an essential gene (Stukey et al., 1989), knockout of *OLE1* cannot be carried out to mimic the decrease of membrane fluidity found in *opi3*Δ. An increase in MUFAs resulted in the rapid degradation of Sbh1 in WT cells similar to the degradation rate observed in *opi3*Δ (Fig. 3 F). The overexpression of *OLE1* in *opi3*Δ did not restore membrane fluidity (Fig. 3 D, E) and had no significant effect on the stability of Sbh1 (Fig. 3 F). This may be due to other changes

besides saturation which affects the fluidity of the ER membrane in cells under LP such an increase in membrane protein abundance.

Sbh1 dissociates from Sec61 complex under lipid imbalance

To further characterise the effect of LP on Sbh1 stability, we performed split ubiquitin based membrane yeast two hybrid (MYTH) assay in WT and *opi3*Δ cells to identify changes in Sbh1 membrane protein interactome (Paumi et al., 2007; Snider, Kittanakom, Damjanovic, et al., 2010). The bait construct was added at the N-terminus of Sbh1. The reverse tagging at the C-terminus was not carried out as luminal bait is not compatible with the assay. Localisation at the ER of tagged Sbh1 was unaffected in WT and *opi3*Δ (Fig. S5 A). Sbh1 bait strain was transformed with a yeast genomic plasmid library in which ORFs are fused to sequences encoding the prey sequence (Snider, Kittanakom, Curak, et al., 2010). A total of 49 and 14 putative Sbh1-interacting proteins were identified in WT and *opi3*Δ, respectively (Fig. S5 B). To eliminate false positive interactors, we performed the bait dependency test using the single-pass transmembrane domain of human T-cell surface glycoprotein CD4 tagged to Cub-LexA-VP16 MYTH (Snider, Kittanakom, Curak, et al., 2010). In WT, we identified 38 proteins interacting with Sbh1 including previously reported interactors Ost4, Sec61, Spc2, Ssb1, Sss1, and Yop1 (Fig. 4 A) (Babu et al., 2012; Chavan, Yan, & Lennarz, 2005; Panzner, Dreier, Hartmann, Kostka, & Rapoport, 1995; Zhao & Jantti, 2009). Sbh1 was also found to interact with membrane proteins involved in sterol biogenesis (Erg4, Erg24 and Nsg1) and fatty acid elongation (Elo2 and Tsc13). On the other hand, only 13 proteins were found to interact with Sbh1 in *opi3*Δ cells (Fig. 4 B). No interaction of Sbh1 with Sec61 and Sss1 was detected in *opi3*Δ. Thus, failure of Sbh1 to associate to the Sec61 complex under LP might cause its premature degradation. This is consistent with the finding that Sbh2, the homolog of Sbh1, becomes destabilised and degraded rapidly when unbound to the Sec61-like complex Ssh1 (Habeck, Ebner, Shimada-Kreft, & Kreft, 2015). Interestingly, Sbh1 was found to interact with proteins of the ERAD pathway under LP (Fig. 4 B). Sbh1 interactors include the membrane-embedded ubiquitin-protein ligase Doa10 which is part of the ERAD Doa10 complex (Carvalho, Goder, & Rapoport, 2006; Deng & Hochstrasser, 2006). As the Doa10 complex is generally specific for substrates containing cytosolic lesions (ERAD-C) (Vashist & Ng, 2004), it suggests that a polypeptide stretch of Sbh1 might become exposed on its cytosolic side under lipid disequilibrium making it susceptible to ubiquitination. Subsequently, targeted substrates for degradation are polyubiquitylated in the cytosol by the addition

of Lys-11-linked ubiquitin (Ubi4) identified to interact with Sbh1 in *opi3*Δ cells. The AAA$^+$ ATPase protein Cdc48 was also found to interact with Sbh1 in *opi3*Δ cells (Fig. 4 B). Ubiquitylated substrates are retro-translocated to the cytosol by the actin of the Cdc48 complex and targeted to the proteasome for degradation (Braun, Matuschewski, Rape, Thoms, & Jentsch, 2002; Ye, Meyer, & Rapoport, 2001). Another important player of the ERAD pathway, Png1, was found to exclusively interact with Sbh1 under lipid imbalance. Png1 catalyses the deglycosylation of misfolded glycoproteins, and is a critical step for ERAD substrates before degradation (Suzuki, Park, Hollingsworth, Sternglanz, & Lennarz, 2000). Together, the MYTH screening results suggest that a decrease in membrane fluidity leads to the dissociation of Sbh1 from the Sec61 complex, resulting in its rapid degradation through the ERAD-C complex.

To ensure that Sbh1 is destabilised from a change in membrane fluidity and not from the destabilisation of the other proteins in the Sec61 complex under lipid perturbation, we carried out cycloheximide chase assay to follow the stability of Sec61 and Sss1-Flag. Both Sec61 and Sss1 were found to be stable in *opi3*Δ as in WT in agreement with our previously reported proteomic data (Fig. 4 C) (Thibault et al., Mol Cell 2012). To further asses the interaction of Sbh1 with Sec61 complex on the ER membrane, proteins were cross-linked before carrying out co-immunoprecipitation (Fig. 4 D). Proteins in both WT and *opi3*Δ cells were treated with the cross-linker dimethyl dithiobispropionimidate (DTBP) before pulling down Sbh1-HA. DTBP stabilises protein interactions prior to co-immunoprecipitation (co-IP) assay to capture protein interactions before the proteins were extracted. This is particularly important to capture membrane protein interactions from the native lipid environment. Sec61 was found to immunoprecipitate with Sbh1-HA in both WT and *opi3*Δ*,* verifying that Sbh1 can still interact with Sec61 under lipid perturbation. Although contradicting our MYTH screening, the interaction of Sbh1 with Sec61 might be minimal and thus below the threshold to be identified from MYTH assay but sufficient for cross-linked co-IP.

A cytoplasmic stretch of Sbh1 is recognised and degraded by ERAD under lipid imbalance

To further validate that Sbh1 is degraded in a Doa10-dependent manner, we carried out cycloheximide chase assay to monitor Sbh1 stability in different ERAD mutants. Sbh1 was found to be fully stabilised in *opi3*Δ*doa10*Δ but not in *opi3*Δ*hrd1*Δ and *opi3*Δ*usa1*Δ mutants (Fig. 5 A). Hrd1 and Usa1 are both

part of the Hrd1 complex which recognises legions of luminal domains or membrane and soluble proteins (EARD-L) and of lesions within transmembrane domains (ERAD-M) (Thibault & Ng, 2012). As some misfolded proteins in the ER are transported to the vacuole for degradation, we confirmed that Sbh1 degradation is not affected by genetically inhibiting vacuolar protein degradation using *pep4*Δ but showed dependency to Cue1, a conserved element in both the Doa10 and Hrd1 complexes (Fig. S6). Together with the MYTH data, it suggests that Sbh1 is exclusively targeted for degradation by the ERAD Doa10 complex through a cytosolic lesion.

To further elucidate how Sbh1 might be targeted for degradation from the Doa10 complex, we looked into the conservation of the lysine residues of the cytoplasmic domain of Sbh1. We aligned Sbh1 sequences from 90 different eukaryotes (Fig 5B). Lysine 23 and 41 of *S. cerevisiae* Sbh1 were found to be the most conserved, with 48.4% and 39.6% occurrence, respectively. Lysine 23 was reported to be a likely site for ubiquitination together with lysine 31 (Swaney et al., 2013). We mutated a key Sbh1 lysine residue that is near the ER membrane on the cytosolic site. The lysine at position 41 was mutated [Sbh1(K41A)] as its exposure to E3 ligase Doa10 might be prolonged in *opi3*Δ cells due to a decrease in membrane fluidity. Additionally, the shortening of the fatty acid chain of the ER (Fig. 3 A) can result in an increase in exposure of the lysine residue. As expected, Sbh1(K41A) was significantly stabilised compared to Sbh1 in *opi3*Δ cells (Fig. 5 C). In WT cells, no significant changes were observed in the stability of Sbh1(K41A) compared to Sbh1. This suggest that a degradation motif of TPs might become accessible to E3 ligases during LP leading to their premature degradation.

We have previously reported protein biogenesis defects of CPY and Gas1 in cells under LP without the intervention of the UPR (Thibault et al., 2012). Surprisingly, protein analyses revealed Sbh1 as the only protein candidate to have a lower abundance under LP in the co-translational and post-translational translocation complex. Hence, we wanted to validate whether low abundance of Sbh1 can lead to the translocation defect of CPY found in LP. Translocation efficiency can be monitored *in vivo* by the shift in mobility reflecting the addition of N-linked glycans in the ER. We confirmed that the absence of Sbh1 causes a defect in translocation from the accumulation of pre-CPY in both *sbh1*Δ and *ire1*Δ*sbh1*Δ mutants (Fig 5D). As the UPR is muted in *ire1*Δ, this suggests that the UPR is unable to intervene to fix the translocation defect of CPY in *sbh1*Δ. We verified that *sbh1*Δ mutant did not lead to ER stress using

a β-galactosidase reporter assay to measure UPR activation (Fig. S7). The overexpression of the other components of the post-translational translocation complex by the UPR is sufficient to overcome the delay in translocation in *opi3*Δ and *opi3*Δ*sbh1*Δ mutants. This suggests that low abundance of Sbh1 under LP can result in the translocation defect seen in cells under LP. Taken together, our data suggest that Sbh1 dissociates from the Sec61 complex causing it to be prematurely ubiquitylated by the Doa10 complex (Fig 5E). This targeting by the ERAD complex leads to Sbh1 degradation by the proteasome resulting in translocation defect of Sbh1-depleted Sec61 complexes.

DISCUSISON

The strong association between obesity and non-alcoholic fatty liver disease (NAFLD) in human populations is evident of the importance of lipid regulation in determining the emergence of fatty liver pathogenesis: NAFLD is now the most common cause of chronic liver enzyme elevations and cryptogenic cirrhosis, as a result of increased obesity (Doycheva et al., 2017; Malhotra & Beaton, 2015). Total PC decreases consistently in NAFLD and NASH livers from human patients and mouse models (Puri et al., 2007; D. E. Vance, 2014; Wattacheril et al., 2013) and it correlates with a decrease of the enzyme required for *de novo* synthesis of PC in the liver, PEMT (Fu et al., 2011; Wattacheril et al., 2013). Concurrently, chronic ER stress and the activation of the UPR are both associated with NAFLD pathologies (Fu et al., 2011; Puri et al., 2008; Yang, Li, Fu, Calay, & Hotamisligil, 2010). Despite these connections, little is known on the effect of phospholipid perturbation on pathways of the ER. Thus, we sought to better understand how the ER fails to reach homeostasis under chronic PC depletion using our previously reported yeast model system (Thibault et al., 2012).

Previously, we reported a remodelling of the proteostasis network that occurs upon PC depletion in yeast (Thibault et al., 2012). Although a large subset of proteins is increased in these stressed cells, we noticed that some key proteins are rapidly degraded and are indeed sensitive to phospholipid variations. Out of the 66 proteins which displayed decreased protein abundance despite being genetically upregulated, 40% are transmembrane proteins (TPs). As 30% of the proteome is predicted to be integral or peripheral membrane proteins (Babu et al., 2012), it suggests that TPs are more sensitive to lipid perturbation compared to other type of proteins. Among the identified TPs, a large proportion are ER-resident proteins suggesting the vulnerability of the organelle to maintain TPs

integrity. The virtual absence of sterols at the ER, a key regulator of membrane fluidity, might contribute to its susceptibility to change in the biophysical properties of the membrane through lipid variation (Zinser, Paltauf, & Daum, 1993)Weete et al., 2010; (Subczynski, Pasenkiewicz-Gierula, Widomska, Mainali, & Raguz, 2017).

We sought to investigate the changes in membrane properties under LP that caused the destabilisation of a subset of TPs. PC is cylindrically shaped with a cross-sectional area for the head group similar to acyl chain tails, generating minimal curvature and forming flat lamellar phase phospholipid bilayers (Szule, Fuller, & Rand, 2002). PE is classified as cone-shaped lipid forming non-lamellar membrane structure as it generates negative membrane curvature (J. E. Vance & Tasseva, 2013). The phospholipid intermediate MMPE becomes highly abundant under the ablation of *OPI3*, and being mono-methylated, it has physical properties similar to PE (Fig. 1 A). The increase in membrane curvature from the replacement of PC to MMPE may induce cells to decrease their fatty acid chain lengths in accordance to the seminal Helfrich theory of membrane bending elasticity (Fig. 3 A; (Zimmerberg & Kozlov, 2006). A larger remodelling of the fatty acid chain length in the ER over whole cell suggests either the ER is more susceptible to LP due to the minimal presence of ergosterol at the ER (Zinser et al., 1993) or cells respond more aggressively to the ER membrane bilayer disruption to alleviate ER stress. Accordingly, a rise in membrane lipid packing from elevated saturated fatty acids will reduce the potency to form curvatures (Fig. 3 B).

The remodelling of the ER to alleviate negative membrane curvature stress, induced from high PE and MMPE levels, can impose further challenges to cells. An elevation in saturated fatty acid chains decreases ER membrane fluidity (Fig. 3 B and D;(Mansilla, Cybulski, Albanesi, & de Mendoza, 2004)) which might be partially due to the absence of the rich unsaturated fatty acid provider, PC (Holthuis & Menon, 2014; Pineau et al., 2008). Additionally, the replacement of PC with MMPE contributes to the stiffening of the membrane (Dawaliby et al., 2016). Thus, these changes combined with the relatively low abundance of ergosterol at the ER membrane bilayer make this organelle particularly susceptible to variation into the most abundant phospholipid, phosphatidylcholine.

Membrane properties impact both protein-protein interactions and protein-lipid interface (Contreras, Ernst, Wieland, & Brugger, 2011). Indeed, known Sbh1 interactors were lost under LP including the other two members of the Sec61 complex, Sec61 and Sss1 (Fig. 4, A and B). The loss of Sbh1 interaction to the Sec61 complex supports its susceptibility to be prematurely degraded as its assembly to the complex promotes folding and stability (Christis, Lubsen, & Braakman, 2008). Similarly, Sbh2, the homolog of Sbh1, is rapidly degraded when dissociated to the Ssh1 complex (Habeck et al., 2015). However, Sbh1 is not required for the stability of Sec61 in complex with Sss1 (Fig. 4 C). In contrast, Sbh1 was found to interact with Sec61 by cross-linked co-IP. This might be due to new electrostatic or hydrophobic attraction from introducing the cross-linker DTBP (Kluger & Alagic, 2004). Sbh1 interaction to the Sec61 complex under LP, suggests that changes in the lipid biophysical properties and not Sbh1 protein conformation results in the loss of interaction of Sbh1 with the Sec61 complex.

Alteration of lipid raft composition at the plasma membrane can lead to loss of protein function and rapid degradation (Lauwers, Grossmann, & Andre, 2007; Payet et al., 2013; Pineau et al., 2008). Likewise, alteration of ER membrane lipid integrity promotes Sbh1 degraded in a Doa10-dependent manner through the ubiquitination of Sbh1 cytosolic lysine at position 41 (Fig. 4 B and Fig. 5 A and C; (Carvalho et al., 2006)). The rigidity of the ER membrane, from depleting PC, may interfere with Sbh1 conformational changes necessary for its interaction with Sec61 complex and thus will result in its degradation (Babst, 2014). Alternatively, the stiffening of the lipid membrane may reduce Sbh1 lateral and transversal diffusion through the lipid bilayer leading to longer interaction with the Doa10 complex (Fig. 3 and Fig. 5, (Ginsberg, Brown, Simon, & Spector, 1981)). It is also reasonable to speculate that the E3 ubiquitin-protein ligase Doa10 might recognise an intermembrane degron of Sbh1 as previously reported for its homolog Sbh2 (Habeck et al., 2015). Thus, a decrease of PC clearly targets Sbh1 for degradation from a change in the biophysical property of the membrane (Fig. 5 E). It remains to be determined if Sbh1 degradation mechanism from LP applies to other unstable TPs identified (Fig. 1 B). Additionally, the absence of PC large head-group and the abnormally high presence of PE and MMPE smaller head-groups at the lipid-cytosol interface should result in an increase in exposure of Sbh1 lysine 41 to Doa10.

The coordinated upregulation of the proteostasis network by the UPR serves as an important stress recovery mechanism that helps cells cope to the otherwise lethal effects of LP (Thibault et al., 2012). Despite this robust stress response under LP, the UPR programme fails to increase the expression level of a subset of TPs (Fig. 1 C). The premature degradation of these TPs can prevent an effective proteostatic response especially under prolonged LP (Fig. 6). ER stress induced from a temporary lipid perturbation will result in the upregulation of UPR target genes and consequently ER homeostasis. However, in the context of fatty liver, prolonged LP might prevent cells to reach ER homeostasis from the premature degradation of some key UPR target TPs. Therefore, this will lead to chronic ER stress which might contribute to the progression of NAFLD. The prolonged upregulation of lipogenic transcription factors from the UPR programme may also contribute to liver progression into hepatosteatosis (Malhi & Kaufman, 2011).

In contrast, disrupting phospholipid homeostasis may be exploited to target pathogens. An increase in phospholipid synthesis is essential for *Plasmodium falciparum*'s cell division during the red blood cell cycle stage (Bobenchik et al., 2010). Phospholipid content of malaria-infected erythrocytes dramatically increases during maturation with 85% of newly phospholipids synthesised being PC and PE for growth and cell division (Holz, 1977). Hence, the inhibition of phospholipid synthesis might be an effective strategy for antimalarial drugs (Bobenchik et al., 2010; Pessi & Ben Mamoun, 2006). In addition, *P. falciparum* resistance to artemisinin-based combination therapies (ACTs) is associated to ER stress where the UPR mitigates artemisinin-induced protein damage (Mok et al., 2015). Thus, targeting phospholipid biosynthesis in combination with artemisinin might be an efficient strategy to overcome resistance by preventing effective UPR activation in *P. falciparum*. (Ben Mamoun, Prigge, & Vial, 2010). Similarly, it might be applied to diseases such as cancer where UPR activation promotes cell division (Bi et al., 2005; Wu et al., 2014).

MATERIALS AND METHODS

Statistics

Error bars indicate standard error of the mean (SEM), calculated from at least three biological replicates, unless otherwise indicated. *P* values were calculated using two-tailed Student's t test, unless otherwise indicated, and reported as *P*=value in figures.

Strains and antibodies

Saccharomyces cerevisiae strains used in this study are listed in Table S2. Strains were generated using standard cloning protocols. Anti-Kar2 polyclonal rabbit antibody and anti-Sec61 polyclonal rabbit antibody were gifts from Davis Ng (Temasek Life Sciences Laboratories, Singapore). Anti-HA mouse monoclonal antibody HA.11 (Covance, Princeton, NJ), anti-Pgk1 mouse monoclonal antibody (Invitrogen), anti-tubulin mouse monoclonal antibody 12G10 (DHSB) and anti-LexA polyclonal rabbit antibody (Abcam, Cambridge, United Kingdom) were commercially purchased. Secondary antibodies goat anti-mouse IgG-DyLight 488 (Thermo Fisher, Waltham, MA), anti-rabbit IgG-DyLight 550 (Thermo Fisher, Waltham, MA), goat anti-mouse IgG-HRP (Santa Cruz Biotechnology, Dallas, TX), goat anti-rabbit IgG-HRP (Santa Cruz Biotechnology, Dallas, TX), goat anti-mouse IgG-IRDye 800 (LI-COR Biosciences) and goat anti-rabbit IgG-IRDye 680 (LI-COR Biosciences, Lincoln, NE) were commercially purchased.

Plasmids used in this study

Plasmids and primers used in this study are listed in Table S3 and S4, respectively. Plasmids were constructed using standard cloning protocols. All coding sequences of constructs used in this study were sequenced in their entirety. The plasmid pGT0179, pGT0181, pGT0183, and pGT0185, were generated by amplifying the promoter, open reading frame, and terminator of *NSG2*, *CUE1*, *SBH1*, and *EMC4* with primer pairs BN033-034, BN029-030, BN035-036, and BN031-032, respectively, from the template WT genomic DNA (gDNA). PCR products of *NSG2, SBH1,* and *EMC4* were digested with the restriction enzymes *NotI* and *NcoI* before being ligated into the corresponding restriction sites in pRS315. *CUE1* PCR product was digested with the restriction enzymes *NotI* and *PstI* before being ligated into the corresponding restriction sites in pRS315. The plasmid pGT0288 was generated by amplifying the open reading frame of Sbh1 with primer BN027 and BN028 from WT gDNA and digested with the restriction enzyme *Sfi1* before being ligated into the corresponding restriction sites in pBT3N. The plasmid pGT0349 was generated by Gibson assembly to join promoter of *PRC1* and open reading frame of *OLE1* generated with primers BN001 and BN002 from WT gDNA with a 3X FLAG tag amplified with primers BN015 and BN016 from pGT0284 into pRS313. The plasmid pGT0352 was generated by performing a site directed mutagenesis with primer BN037 and BN038 on pGT0183 as previously described (Nelson, Lawson, Klingenberg, & Douglas, 1993). The plasmid pGT0350 was generated by

Gibson assembly to join the promoter and open reading frame of *SSS1* with primers BN013 and BN014 from WT gDNA with a 3X FLAG tag amplified with primers BN015 and BN016 from pGT0284 into pRS313.

Cycloheximide chase assay

Cycloheximide chase assay was carried out as previously described (Prasad, Kawaguchi, & Ng, 2010). Typically, 6 OD_{600} units of early log phase cells were grown in synthetic media. Protein synthesis was inhibited by adding 200 µg/ml cycloheximide. Samples were taken at designated time points. Cell lysates from these samples were resolved by SDS-PAGE and transferred onto a nitrocellulose membrane. Immunodetection was performed with appropriate primary antibodies and horseradish peroxidase-conjugated secondary antibodies or IRDye-conjugated secondary antibodies. Proteins were visualised using the ECL system (C-DiGit Chemiluminescent Western Blot Scanner) or the NIR fluorescence system (Odyssey CLx Imaging System). Values for each time point were normalised using anti-Pgk1 or anti-Tub1 as loading controls. Quantification was performed using an Odyssey infrared imaging program (LI-COR Biosciences, Lincoln, NE).

Indirect immunofluorescence

Indirect immunofluorescence was carried out as previously described (Spear & Ng, 2003). Typically, cells were grown to early log phase at 30°C in selective synthetic complete media, fixed in 10% formaldehyde and permeabilised. After blocking with 3% BSA, staining was performed using anti-HA (1:200) and anti-Kar2p primary antibody (1:1,000) followed by Alexa Fluor 488 goat anti-rabbit secondary antibody (1:1,000). Samples were visualised using a Zeiss LSM 710 microscope with a 100x 1.4 NA oil Plan-Apochromat objective (Carl Zeiss MicroImaging).

Alkaline carbonate extraction

Alkaline Carbonate Extraction was carried out as previously described (S. Wang, Thibault, & Ng, 2011). Five OD_{600} of early log phase cells were resuspended in 1.2 ml of 10 mM sodium phosphate pH 7.0, 1mM PMSF and protease inhibitor cocktail (PIC). Equal volume of 0.2 M sodium carbonate (pH 11.0) was added to cell lysates incubated 30 min at 4°C and spun down at 100,000 x *g* for 30 min, 4°C. The pellet (membrane fraction) was solubilised in 3% SDS, 100 mM Tris, pH 7.4, 3 mM DTT and incubated

at 100°C for 10 min. Total lysate and supernatant (collected from centrifuged lysate) were precipitated with 10% trichloroacetic acid (TCA) and spun down 30 min at 18,400 x *g*, 4°C. Proteins were resuspended in TCA resuspension buffer (100 mM Tris-HCL pH 11.0, 3% SDS).

Proteinase K digestion assay

Fifty OD_{600} units of early log phase cells were pelleted and resuspended in 1 ml Tris Buffer (50 mM Tris pH 7.4, 50 mM NaCl, 10% glycerol, 1mM PMSF and PIC). Clarified cell lysate was spun down at 100,000 x *g* for 1 h at 4 °C. The pellet was resuspended and washed with 0.5 ml Tris Buffer without PMSF and PIC. Around ~ 5 OD_{600} equivalent of microsomes were incubated with 1 mg/ml Proteinase K (Promega, Fitchburg, WI) and 1% Nonidet P40 substitute (Sigma-Aldrich, St. Louis, MO) when indicated and incubated at 37°C for 30 min. To quench the reaction, 5 mM PMSF was added followed by TCA precipitation. Samples were resolved by SDS-PAGE and transferred onto a nitrocellulose membrane. Immunodetection was performed with appropriate primary antibodies and IRDye-conjugated secondary antibodies. Immunoreactive species were visualised using the NIR fluorescence system (Odyssey CLx Imaging System).

Lipid extraction and fatty acid analysis

For whole cells, 10 OD_{600} of early log phase cells were pelleted, washed and resuspended with ice-cold water and lyophilised using Virtis Freeze Dryer under vacuum. For lipid extraction for microsomes, 50 OD_{600} of early log phase cells were pelleted, washed with phosphate-buffered saline (PBS) and resuspended in 1 ml of Tris Buffer (50 mM Tris-HCL, 150 mM NaCl, 5 mM EDTA pH 8.0, 167 µM PMSF and PIC). Clarified lysate was spun down at 100,000 x *g* for 1 h at 4°C. The pellet was resuspended in 100 µl ddH_2O and sonicated for 30 min. Lipid content was normalised to protein content using bicinchoninic acid (BCA) protein assay (Sigma-Aldrich, St. Louis, MO). Normalised microsome contents were resuspended with ice-cold ddH_2O and lyophilised using Virtis Freeze Dryer under vacuum. Lyophilised samples were subjected to 300 µl 1.25 M HCl-MeOH (Sigma-Aldrich, St. Louis, MO) and incubated at 80°C for 1 h to hydrolyse and esterify FAs into FA methyl ester (FAME). FAME were extracted three times with 1 ml of hexane and separated on a gas chromatography with flame ionization detector (GC-FID; GC-2014; Shimadzu, Kyoto, Japan) equipped with an Ulbon HR-SS-10 capillary column (nitrile silicone, 25 m x 0.25 mm; Shinwa Chemical Industries, Kyoto, Japan). The temperature

was held 3 min at 160°C and increase to 180°C with 1.5°C/min increments and to 220°C with 4°C/min increments.

Fluorescent recovery after photobleaching

Fluorescent recovery after photobleaching (FRAP) was carried out as previously described (Shibata et al., 2008). Typically, early log phase cells expressing Sec63-GFP were fixed on coverslips in Attofluor cell chamber (Thermo Fisher, Waltham, MA) with Concanavalin A before rinsing thrice with ddH_2O. Cells were imaged for 5 s followed by photobleaching a region of interest of 82 x 82 pixels at 100% intensity 488 nm laser under 5x magnification. Subsequently, images were taken at 1.57 sec intervals for a total of 160 sec. Images were acquired using a Zeiss LSM 710 microscope with a 100x 1.4 NA oil Plan-Apochromat objective (Carl Zeiss MicroImaging) with argon laser line 488 nm of optical slices 4.2 µm. ZEN black edition was used for image acquisition and analysis. Magnification, laser power, and detector gains were identical across samples. For data analysis, the fluorescence intensity of three regions of interest was measured for the entire course of the experiment: the region of interest (ROI), a region outside of the cell to measure the overall background fluorescence (BG), and a non-photobleached region within the cell was monitored to measure the overall photobleaching and fluorescence variation (REF). Normalised fluorescence intensity [$F(t)_{norm}$] was calculated for each time point using Eq. 1 (Day, Kraft, Kang, & Kenworthy, 2012). F(i) denotes the initial fluorescence intensities.

$$F(t)_{norm} = \frac{F(t)_{ROI} - F_{BG}}{F(t)_{REF} - F_{BG}} \times \frac{F(i)_{REF} - F_{BG}}{F(i)_{ROI} - F_{BG}} \qquad (1)$$

Fluorescent recovery was analysed by calculating half fluorescent intensity ($t_{½}$) using Eq. 2 (Feder, Brust-Mascher, Slattery, Baird, & Webb, 1996). F_0 denotes the normalised initial fluorescence intensity, F_∞ the normalised maximum fluorescence intensity and F(t) the normalised fluorescent intensity at each time point.

$$F(t) = \frac{F_0 + F_\infty \frac{t}{t_{1/2}}}{1 + \frac{t}{t_{1/2}}} \qquad (2)$$

The $t_{½}$ values were plotted using GraphPad Prism 5.0.

Membrane yeast two-hybrid system assay

Membrane yeast two-hybrid (MYTH) assay was carried out as previously described (Snider, Kittanakom, Damjanovic, et al., 2010). Yeast two-hybrid screen uses the split ubiquitin two hybrid (N-terminus, Nub and C-terminus, Cub). Briefly, MYTH bait was generated by integrating Cub-LexA-VP16 tag at the N-terminus of Sbh1 under the control of the promoter *CYC1* and transformed in NMY51 strain. Sbh1 tagged protein localization was verified by indirect immunofluorescence using anti-LexA antibodies against the tag as describe above. Seven µg of NubG-X cDNA prey library (Dualsystems) was transformed in 35 OD_{600} unit of *SBH1* reporter strain. Interactors were isolated on selective complete (SC) media lacking tryptophan, leucine, adenine and histidine complemented with 80 µg/mL X-Gal and 5 mM 3-Amino-1,2,4-triazole (3-AT) and grown for two days at 30°C. The histidine inhibitor 3-AT was used to reduce false positive colonies. Only colonies which display robust growth on selective media and a blue colour were selected for further analysis. The prey cDNA plasmids were isolated and sequenced. The list of interactors was verified via the Bait Dependency Test, where all of the identified interactors are retransformed back into the original bait strain, together with a negative control using the single-pass transmembrane domain of human T-cell surface glycoprotein CD4 tagged to Cub-LexA-VP16 MYTH (Snider, Kittanakom, Curak, et al., 2010). Yeast carrying the artificial bait and prey which cause activation of the reporter system, were removed from the list of interactors. Yeast that harbour the prey and the bait-of-interest and did not grow were likewise removed from the list of interactors.

Co-immunoprecipitation

Co-immunoprecipitation was carried out as previously described (Xu & Reed, 1998). Briefly, thirty OD_{600} unit of early log phase cells were incubated with 100 µg/ml dimethyl 3,3′-dithiopropionimidate dihydrochloride (DTBP) for 30 min at RT and stopped with ice-cold 50 mM TBS with 0.1% Tween 20. Cells were resuspended in 700 µl Tris buffer (50 mM Tris-HCl pH 7.9, 5 mM EDTA, 150 mM NaCl, 1% Triton X-100, mM PMSF and PIC). Clarified cell lysate was incubated with Protein G beads and anti-HA antibodies overnight at 4°C. Beads were washed thrice with Tris buffer and twice with TBS. Proteins were separated using SDS-PAGE and visualised by immunoblot as described above.

Cell Labelling and immunoprecipitation

Cell labelling and immunoprecipitation was carried out as previously described (Thibault et al., 2011). In brief, three OD_{600} units of early log phase cells were labelled with 80 µCi of L-[^{35}S]-methionine/cysteine mix (Perkin Elmer) for 5 minutes. A chase was carried out with the addition of cold methionine/cysteine (2 mM final concentration) and samples were taken at designated time points. Cell lysates from these samples were then subjected to immunoprecipitation with the appropriate antiserum, resolved by SDS-PAGE and visualised using a Typhoon TRIO phosphorimager (Amersham).

β-galactosidase reporter assay

The β-galactosidase reporter assay was carried out as previously described (Thibault et al., 2011). Typically, 4 OD_{600} units of early log phase cells were collected and resuspended in 75 µl LacZ buffer (125 mM sodium phosphate, pH 7, 10 mM KCl, 1 mM $MgSO_4$, 50 mM β-mercaptoethanol). As positive control to induce the UPR, tunicamycin was added at a concentration of 2.5 µg/ml to growing WT cells 1h prior to harvest. An aliquot of 25 µl cell resuspension was transferred into 975 µl ddH_2O and the absorbance was measured at 600 nm. To the remaining resuspension, 50 µl chloroform and 20 µl 0.1% SDS were added and vortexed vigorously for 20 sec. The reaction was started with the addition of 1.4 mg/ml ONPG (2-nitrophenyl -D-galactopyranoside; Sigma) in LacZ buffer. Then, the reaction was stopped with 500 µl of 1 M Na_2CO_3 when sufficient yellow colour had developed without exceeding a ten-minute reaction. The absorbance was measured at 420 and 550 nm. The β-galactosidase activity was calculated using Eq. (3).

$$\text{Miller units} = 1000 \times (OD_{420} - 1.75 \times OD_{550})/(t \times (VA/VR) \times OD_{600}) \quad (3)$$

The values were then normalised to the activity of WT.

ACKNOWLEDGEMENTS

We are grateful to Davis Ng for providing reagents. We thank Chengchao Xu and members of Thibault lab for critical reading of the manuscript. This work was supported by the Nanyang Assistant Professorship program from Nanyang Technological University and the Nanyang Technological University Research Scholarship to B. S.H. N. and P.J.S. (predoctoral fellowship).

COMPETING INTERESTS

The authors declare that they have no conflict of interest.

REFERENCES

Arendt, B. M., Ma, D. W., Simons, B., Noureldin, S. A., Therapondos, G., Guindi, M., . . . Allard, J. P. (2013). Nonalcoholic fatty liver disease is associated with lower hepatic and erythrocyte ratios of phosphatidylcholine to phosphatidylethanolamine. *Appl Physiol Nutr Metab, 38*(3), 334-340. doi:10.1139/apnm-2012-0261

Babst, M. (2014). Quality control: quality control at the plasma membrane: one mechanism does not fit all. *J Cell Biol, 205*(1), 11-20. doi:10.1083/jcb.201310113

Babu, M., Vlasblom, J., Pu, S., Guo, X., Graham, C., Bean, B. D., . . . Greenblatt, J. F. (2012). Interaction landscape of membrane-protein complexes in Saccharomyces cerevisiae. *Nature, 489*(7417), 585-589. doi:10.1038/nature11354

Ben Mamoun, C., Prigge, S. T., & Vial, H. (2010). Targeting the Lipid Metabolic Pathways for the Treatment of Malaria. *Drug Dev Res, 71*(1), 44-55. doi:10.1002/ddr.20347

Bi, M., Naczki, C., Koritzinsky, M., Fels, D., Blais, J., Hu, N., . . . Koumenis, C. (2005). ER stress-regulated translation increases tolerance to extreme hypoxia and promotes tumor growth. *EMBO J, 24*(19), 3470-3481. doi:10.1038/sj.emboj.7600777

Biederer, T., Volkwein, C., & Sommer, T. (1997). Role of Cue1p in ubiquitination and degradation at the ER surface. *Science, 278*(5344), 1806-1809.

Bobenchik, A. M., Choi, J. Y., Mishra, A., Rujan, I. N., Hao, B., Voelker, D. R., . . . Ben Mamoun, C. (2010). Identification of inhibitors of Plasmodium falciparum phosphoethanolamine methyltransferase using an enzyme-coupled transmethylation assay. *Bmc Biochemistry, 11*. doi:Artn 410.1186/1471-2091-11-4

Boumann, H. A., Gubbens, J., Koorengevel, M. C., Oh, C. S., Martin, C. E., Heck, A. J., . . . de Kroon, A. I. (2006). Depletion of phosphatidylcholine in yeast induces shortening and increased saturation of the lipid acyl chains: evidence for regulation of intrinsic membrane curvature in a eukaryote. *Mol Biol Cell, 17*(2), 1006-1017. doi:10.1091/mbc.E05-04-0344

Braun, S., Matuschewski, K., Rape, M., Thoms, S., & Jentsch, S. (2002). Role of the ubiquitin-selective CDC48(UFD1/NPL4)chaperone (segregase) in ERAD of OLE1 and other substrates. *EMBO J, 21*(4), 615-621.

Buang, Y., Wang, Y. M., Cha, J. Y., Nagao, K., & Yanagita, T. (2005). Dietary phosphatidylcholine alleviates fatty liver induced by orotic acid. *Nutrition, 21*(7-8), 867-873. doi:10.1016/j.nut.2004.11.019

Carman, G. M., & Henry, S. A. (1989). Phospholipid biosynthesis in yeast. *Annu Rev Biochem, 58*, 635-669. doi:10.1146/annurev.bi.58.070189.003223

Carvalho, P., Goder, V., & Rapoport, T. A. (2006). Distinct ubiquitin-ligase complexes define convergent pathways for the degradation of ER proteins. *Cell, 126*(2), 361-373. doi:10.1016/j.cell.2006.05.043

Chapman, R. E., & Walter, P. (1997). Translational attenuation mediated by an mRNA intron. *Current Biology, 7*(11), 850-859.

Chavan, M., Yan, A., & Lennarz, W. J. (2005). Subunits of the translocon interact with components of the oligosaccharyl transferase complex. *J Biol Chem, 280*(24), 22917-22924. doi:10.1074/jbc.M502858200

Christis, C., Lubsen, N. H., & Braakman, I. (2008). Protein folding includes oligomerization - examples from the endoplasmic reticulum and cytosol. *FEBS J, 275*(19), 4700-4727. doi:10.1111/j.1742-4658.2008.06590.x

Contreras, F. X., Ernst, A. M., Wieland, F., & Brugger, B. (2011). Specificity of intramembrane protein-lipid interactions. *Cold Spring Harb Perspect Biol, 3*(6). doi:10.1101/cshperspect.a004705

Corbin, K. D., & Zeisel, S. H. (2012). Choline metabolism provides novel insights into nonalcoholic fatty liver disease and its progression. *Curr Opin Gastroenterol, 28*(2), 159-165. doi:10.1097/MOG.0b013e32834e7b4b

Costanzo, M., Baryshnikova, A., Bellay, J., Kim, Y., Spear, E. D., Sevier, C. S., . . . Boone, C. (2010). The genetic landscape of a cell. *Science, 327*(5964), 425-431. doi:10.1126/science.1180823

Cox, J. S., Shamu, C. E., & Walter, P. (1993). Transcriptional Induction of Genes Encoding Endoplasmic-Reticulum Resident Proteins Requires a Transmembrane Protein-Kinase. *Cell, 73*(6), 1197-1206. doi:Doi 10.1016/0092-8674(93)90648-A

Dawaliby, R., Trubbia, C., Delporte, C., Noyon, C., Ruysschaert, J. M., Van Antwerpen, P., & Govaerts, C. (2016). Phosphatidylethanolamine Is a Key Regulator of Membrane Fluidity in Eukaryotic Cells. *Journal of Biological Chemistry, 291*(7), 3658-3667. doi:10.1074/jbc.M115.706523

Day, C. A., Kraft, L. J., Kang, M., & Kenworthy, A. K. (2012). Analysis of protein and lipid dynamics using confocal fluorescence recovery after photobleaching (FRAP). *Curr Protoc Cytom, Chapter 2*, Unit2 19. doi:10.1002/0471142956.cy0219s62

Deng, M., & Hochstrasser, M. (2006). Spatially regulated ubiquitin ligation by an ER/nuclear membrane ligase. *Nature, 443*(7113), 827-831. doi:10.1038/nature05170

Doycheva, I., Watt, K. D., Rifai, G., Abou Mrad, R., Lopez, R., Zein, N. N., . . . Alkhouri, N. (2017). Increasing Burden of Chronic Liver Disease Among Adolescents and Young Adults in the USA: A Silent Epidemic. *Dig Dis Sci, 62*(5), 1373-1380. doi:10.1007/s10620-017-4492-3

Dumas, M. E., Barton, R. H., Toye, A., Cloarec, O., Blancher, C., Rothwell, A., . . . Nicholson, J. K. (2006). Metabolic profiling reveals a contribution of gut microbiota to fatty liver phenotype in insulin-resistant mice. *Proc Natl Acad Sci U S A, 103*(33), 12511-12516. doi:10.1073/pnas.0601056103

Feder, T. J., Brust-Mascher, I., Slattery, J. P., Baird, B., & Webb, W. W. (1996). Constrained diffusion or immobile fraction on cell surfaces: a new interpretation. *Biophys J, 70*(6), 2767-2773. doi:10.1016/S0006-3495(96)79846-6

Fei, W., Shui, G., Zhang, Y., Krahmer, N., Ferguson, C., Kapterian, T. S., . . . Yang, H. (2011). A role for phosphatidic acid in the formation of "supersized" lipid droplets. *PLoS Genet, 7*(7), e1002201. doi:10.1371/journal.pgen.1002201

Feng, D., Zhao, X., Soromani, C., Toikkanen, J., Romisch, K., Vembar, S. S., . . . Jantti, J. (2007). The transmembrane domain is sufficient for Sbh1p function, its association with the Sec61 complex, and interaction with Rtn1p. *J Biol Chem, 282*(42), 30618-30628. doi:10.1074/jbc.M701840200

Flury, I., Garza, R., Shearer, A., Rosen, J., Cronin, S., & Hampton, R. Y. (2005). INSIG: a broadly conserved transmembrane chaperone for sterol-sensing domain proteins. *EMBO J, 24*(22), 3917-3926. doi:10.1038/sj.emboj.7600855

Fu, S., Yang, L., Li, P., Hofmann, O., Dicker, L., Hide, W., . . . Hotamisligil, G. S. (2011). Aberrant lipid metabolism disrupts calcium homeostasis causing liver endoplasmic reticulum stress in obesity. *Nature, 473*(7348), 528-531. doi:10.1038/nature09968

Ginsberg, B. H., Brown, T. J., Simon, I., & Spector, A. A. (1981). Effect of the membrane lipid environment on the properties of insulin receptors. *Diabetes, 30*(9), 773-780.

Habeck, G., Ebner, F. A., Shimada-Kreft, H., & Kreft, S. G. (2015). The yeast ERAD-C ubiquitin ligase Doa10 recognizes an intramembrane degron. *J Cell Biol, 209*(4), 621. doi:10.1083/jcb.20140808804292015c

Harding, H. P., Zhang, Y., & Ron, D. (1999). Protein translation and folding are coupled by an endoplasmic-reticulum-resident kinase. *Nature, 397*(6716), 271-274. doi:10.1038/16729

Holthuis, J. C., & Menon, A. K. (2014). Lipid landscapes and pipelines in membrane homeostasis. *Nature, 510*(7503), 48-57. doi:10.1038/nature13474

Holz, G. G., Jr. (1977). Lipids and the malarial parasite. *Bull World Health Organ, 55*(2-3), 237-248.

Jacobs, R. L., Zhao, Y., Koonen, D. P., Sletten, T., Su, B., Lingrell, S., . . . Vance, D. E. (2010). Impaired de novo choline synthesis explains why phosphatidylethanolamine N-methyltransferase-deficient mice are protected from diet-induced obesity. *J Biol Chem, 285*(29), 22403-22413. doi:10.1074/jbc.M110.108514

Jonikas, M. C., Collins, S. R., Denic, V., Oh, E., Quan, E. M., Schmid, V., . . . Schuldiner, M. (2009). Comprehensive characterization of genes required for protein folding in the endoplasmic reticulum. *Science, 323*(5922), 1693-1697. doi:10.1126/science.1167983

Kim, Y. J., Lee, H. S., Kim, Y. K., Park, S., Kim, J. M., Yun, J. H., . . . Kim, B. J. (2016). Association of Metabolites with Obesity and Type 2 Diabetes Based on FTO Genotype. *PLoS One, 11*(6), e0156612. doi:10.1371/journal.pone.0156612

Kluger, R., & Alagic, A. (2004). Chemical cross-linking and protein-protein interactions-a review with illustrative protocols. *Bioorg Chem, 32*(6), 451-472. doi:10.1016/j.bioorg.2004.08.002

Lahiri, S., Chao, J. T., Tavassoli, S., Wong, A. K., Choudhary, V., Young, B. P., . . . Prinz, W. A. (2014). A conserved endoplasmic reticulum membrane protein complex (EMC) facilitates phospholipid transfer from the ER to mitochondria. *PLoS Biol, 12*(10), e1001969. doi:10.1371/journal.pbio.1001969

Lauwers, E., Grossmann, G., & Andre, B. (2007). Evidence for coupled biogenesis of yeast Gap1 permease and sphingolipids: essential role in transport activity and normal control by ubiquitination. *Mol Biol Cell, 18*(8), 3068-3080. doi:10.1091/mbc.E07-03-0196

Li, Z., Agellon, L. B., Allen, T. M., Umeda, M., Jewell, L., Mason, A., & Vance, D. E. (2006). The ratio of phosphatidylcholine to phosphatidylethanolamine influences membrane integrity and steatohepatitis. *Cell Metab, 3*(5), 321-331. doi:10.1016/j.cmet.2006.03.007

Malhi, H., & Kaufman, R. J. (2011). Endoplasmic reticulum stress in liver disease. *J Hepatol, 54*(4), 795-809. doi:10.1016/j.jhep.2010.11.005

Malhotra, N., & Beaton, M. D. (2015). Management of non-alcoholic fatty liver disease in 2015. *World J Hepatol, 7*(30), 2962-2967. doi:10.4254/wjh.v7.i30.2962

Mansilla, M. C., Cybulski, L. E., Albanesi, D., & de Mendoza, D. (2004). Control of membrane lipid fluidity by molecular thermosensors. *J Bacteriol, 186*(20), 6681-6688. doi:10.1128/JB.186.20.6681-6688.2004

Mitsuhashi, S., & Nishino, I. (2011). Phospholipid synthetic defect and mitophagy in muscle disease. *Autophagy, 7*(12), 1559-1561.

Mok, S., Ashley, E. A., Ferreira, P. E., Zhu, L., Lin, Z., Yeo, T., . . . Bozdech, Z. (2015). Drug resistance. Population transcriptomics of human malaria parasites reveals the mechanism of artemisinin resistance. *Science, 347*(6220), 431-435. doi:10.1126/science.1260403

Nelson, D. R., Lawson, J. E., Klingenberg, M., & Douglas, M. G. (1993). Site-directed mutagenesis of the yeast mitochondrial ADP/ATP translocator. Six arginines and one lysine are essential. *J Mol Biol, 230*(4), 1159-1170. doi:10.1006/jmbi.1993.1233

Nicholson, J. K., Holmes, E., Kinross, J., Burcelin, R., Gibson, G., Jia, W., & Pettersson, S. (2012). Host-gut microbiota metabolic interactions. *Science, 336*(6086), 1262-1267. doi:10.1126/science.1223813

Pagliassotti, M. J. (2012). Endoplasmic reticulum stress in nonalcoholic fatty liver disease. *Annu Rev Nutr, 32*, 17-33. doi:10.1146/annurev-nutr-071811-150644

Panzner, S., Dreier, L., Hartmann, E., Kostka, S., & Rapoport, T. A. (1995). Posttranslational protein transport in yeast reconstituted with a purified complex of Sec proteins and Kar2p. *Cell, 81*(4), 561-570.

Paumi, C. M., Menendez, J., Arnoldo, A., Engels, K., Iyer, K. R., Thaminy, S., . . . Stagljar, I. (2007). Mapping protein-protein interactions for the yeast ABC transporter Ycf1p by integrated split-ubiquitin membrane yeast two-hybrid analysis. *Mol Cell, 26*(1), 15-25. doi:10.1016/j.molcel.2007.03.011

Payet, L. A., Pineau, L., Snyder, E. C., Colas, J., Moussa, A., Vannier, B., . . . Ferreira, T. (2013). Saturated fatty acids alter the late secretory pathway by modulating membrane properties. *Traffic, 14*(12), 1228-1241. doi:10.1111/tra.12117

Pessi, G., & Ben Mamoun, C. (2006). Pathways for phosphatidylcholine biosynthesis: targets and strategies for antimalarial drugs. *Future Lipidology, 1*(2), 173-180. doi:10.2217/17460875.1.2.173

Pineau, L., Bonifait, L., Berjeaud, J. M., Alimardani-Theuil, P., Berges, T., & Ferreira, T. (2008). A lipid-mediated quality control process in the Golgi apparatus in yeast. *Mol Biol Cell, 19*(3), 807-821. doi:10.1091/mbc.E07-06-0600

Prasad, R., Kawaguchi, S., & Ng, D. T. (2010). A nucleus-based quality control mechanism for cytosolic proteins. *Mol Biol Cell, 21*(13), 2117-2127. doi:10.1091/mbc.E10-02-0111

Promlek, T., Ishiwata-Kimata, Y., Shido, M., Sakuramoto, M., Kohno, K., & Kimata, Y. (2011). Membrane aberrancy and unfolded proteins activate the endoplasmic reticulum stress sensor Ire1 in different ways. *Mol Biol Cell, 22*(18), 3520-3532. doi:10.1091/mbc.E11-04-0295

Puri, P., Baillie, R. A., Wiest, M. M., Mirshahi, F., Choudhury, J., Cheung, O., . . . Sanyal, A. J. (2007). A lipidomic analysis of nonalcoholic fatty liver disease. *Hepatology, 46*(4), 1081-1090. doi:10.1002/hep.21763

Puri, P., Mirshahi, F., Cheung, O., Natarajan, R., Maher, J. W., Kellum, J. M., & Sanyal, A. J. (2008). Activation and dysregulation of the unfolded protein response in nonalcoholic fatty liver disease. *Gastroenterology, 134*(2), 568-576. doi:10.1053/j.gastro.2007.10.039

Quinn, P. J. (1981). The fluidity of cell membranes and its regulation. *Prog Biophys Mol Biol, 38*(1), 1-104.

Schuldiner, M., Collins, S. R., Thompson, N. J., Denic, V., Bhamidipati, A., Punna, T., . . . Krogan, N. J. (2005). Exploration of the function and organization of the yeast early secretory pathway through an epistatic miniarray profile. *Cell, 123*(3), 507-519. doi:10.1016/j.cell.2005.08.031

Shibata, Y., Voss, C., Rist, J. M., Hu, J., Rapoport, T. A., Prinz, W. A., & Voeltz, G. K. (2008). The reticulon and DP1/Yop1p proteins form immobile oligomers in the tubular endoplasmic reticulum. *J Biol Chem, 283*(27), 18892-18904. doi:10.1074/jbc.M800986200

Snider, J., Kittanakom, S., Curak, J., & Stagljar, I. (2010). Split-ubiquitin based membrane yeast two-hybrid (MYTH) system: a powerful tool for identifying protein-protein interactions. *J Vis Exp*(36). doi:10.3791/1698

Snider, J., Kittanakom, S., Damjanovic, D., Curak, J., Wong, V., & Stagljar, I. (2010). Detecting interactions with membrane proteins using a membrane two-hybrid assay in yeast. *Nat Protoc, 5*(7), 1281-1293. doi:10.1038/nprot.2010.83

Spear, E. D., & Ng, D. T. (2003). Stress tolerance of misfolded carboxypeptidase Y requires maintenance of protein trafficking and degradative pathways. *Mol Biol Cell, 14*(7), 2756-2767. doi:10.1091/mbc.E02-11-0717

Stubbs, C. D. (1983). Membrane fluidity: structure and dynamics of membrane lipids. *Essays Biochem, 19*, 1-39.

Stubbs, C. D., & Smith, A. D. (1984). The modification of mammalian membrane polyunsaturated fatty acid composition in relation to membrane fluidity and function. *Biochim Biophys Acta, 779*(1), 89-137.

Stukey, J. E., McDonough, V. M., & Martin, C. E. (1989). Isolation and characterization of OLE1, a gene affecting fatty acid desaturation from Saccharomyces cerevisiae. *J Biol Chem, 264*(28), 16537-16544.

Subczynski, W. K., Pasenkiewicz-Gierula, M., Widomska, J., Mainali, L., & Raguz, M. (2017). High Cholesterol/Low Cholesterol: Effects in Biological Membranes Review. *Cell Biochem Biophys*. doi:10.1007/s12013-017-0792-7

Suzuki, T., Park, H., Hollingsworth, N. M., Sternglanz, R., & Lennarz, W. J. (2000). PNG1, a yeast gene encoding a highly conserved peptide:N-glycanase. *J Cell Biol, 149*(5), 1039-1052.

Swaney, D. L., Beltrao, P., Starita, L., Guo, A., Rush, J., Fields, S., . . . Villen, J. (2013). Global analysis of phosphorylation and ubiquitylation cross-talk in protein degradation. *Nat Methods, 10*(7), 676-682. doi:10.1038/nmeth.2519

Szule, J. A., Fuller, N. L., & Rand, R. P. (2002). The effects of acyl chain length and saturation of diacylglycerols and phosphatidylcholines on membrane monolayer curvature. *Biophys J, 83*(2), 977-984.

Thibault, G., Ismail, N., & Ng, D. T. (2011). The unfolded protein response supports cellular robustness as a broad-spectrum compensatory pathway. *Proc Natl Acad Sci U S A, 108*(51), 20597-20602. doi:10.1073/pnas.1117184109

Thibault, G., & Ng, D. T. (2012). The endoplasmic reticulum-associated degradation pathways of budding yeast. *Cold Spring Harb Perspect Biol, 4*(12). doi:10.1101/cshperspect.a013193

Thibault, G., Shui, G., Kim, W., McAlister, G. C., Ismail, N., Gygi, S. P., . . . Ng, D. T. (2012). The membrane stress response buffers lethal effects of lipid disequilibrium by reprogramming the protein homeostasis network. *Mol Cell, 48*(1), 16-27. doi:10.1016/j.molcel.2012.08.016

Travers, K. J., Patil, C. K., Wodicka, L., Lockhart, D. J., Weissman, J. S., & Walter, P. (2000). Functional and genomic analyses reveal an essential coordination between the unfolded protein response and ER-associated degradation. *Cell, 101*(3), 249-258.

van Meer, G., Voelker, D. R., & Feigenson, G. W. (2008). Membrane lipids: where they are and how they behave. *Nat Rev Mol Cell Biol, 9*(2), 112-124. doi:10.1038/nrm2330

Vance, D. E. (2014). Phospholipid methylation in mammals: from biochemistry to physiological function. *Biochim Biophys Acta, 1838*(6), 1477-1487. doi:10.1016/j.bbamem.2013.10.018

Vance, J. E., & Tasseva, G. (2013). Formation and function of phosphatidylserine and phosphatidylethanolamine in mammalian cells. *Biochim Biophys Acta, 1831*(3), 543-554. doi:10.1016/j.bbalip.2012.08.016

Vashist, S., & Ng, D. T. (2004). Misfolded proteins are sorted by a sequential checkpoint mechanism of ER quality control. *J Cell Biol, 165*(1), 41-52. doi:10.1083/jcb.200309132

Vevea, J. D., Garcia, E. J., Chan, R. B., Zhou, B., Schultz, M., Di Paolo, G., . . . Pon, L. A. (2015). Role for Lipid Droplet Biogenesis and Microlipophagy in Adaptation to Lipid Imbalance in Yeast. *Dev Cell, 35*(5), 584-599. doi:10.1016/j.devcel.2015.11.010

Volmer, R., & Ron, D. (2015). Lipid-dependent regulation of the unfolded protein response. *Curr Opin Cell Biol, 33*, 67-73. doi:10.1016/j.ceb.2014.12.002

Volmer, R., van der Ploeg, K., & Ron, D. (2013). Membrane lipid saturation activates endoplasmic reticulum unfolded protein response transducers through their transmembrane domains. *Proc Natl Acad Sci U S A, 110*(12), 4628-4633. doi:10.1073/pnas.1217611110

Wang, F., Whynot, A., Tung, M., & Denic, V. (2011). The mechanism of tail-anchored protein insertion into the ER membrane. *Mol Cell, 43*(5), 738-750. doi:10.1016/j.molcel.2011.07.020

Wang, S., Thibault, G., & Ng, D. T. (2011). Routing misfolded proteins through the multivesicular body (MVB) pathway protects against proteotoxicity. *J Biol Chem, 286*(33), 29376-29387. doi:10.1074/jbc.M111.233346

Wattacheril, J., Seeley, E. H., Angel, P., Chen, H., Bowen, B. P., Lanciault, C., . . . Flynn, C. R. (2013). Differential intrahepatic phospholipid zonation in simple steatosis and nonalcoholic steatohepatitis. *PLoS One, 8*(2), e57165. doi:10.1371/journal.pone.0057165

Wu, H., Ng, B. S., & Thibault, G. (2014). Endoplasmic reticulum stress response in yeast and humans. *Biosci Rep, 34*(4). doi:10.1042/BSR20140058

Xu, Q., & Reed, J. C. (1998). Bax inhibitor-1, a mammalian apoptosis suppressor identified by functional screening in yeast. *Mol Cell, 1*(3), 337-346.

Yang, L., Li, P., Fu, S., Calay, E. S., & Hotamisligil, G. S. (2010). Defective hepatic autophagy in obesity promotes ER stress and causes insulin resistance. *Cell Metab, 11*(6), 467-478. doi:10.1016/j.cmet.2010.04.005

Yang, L., Zhao, D., Ren, J., & Yang, J. (2015). Endoplasmic reticulum stress and protein quality control in diabetic cardiomyopathy. *Biochim Biophys Acta, 1852*(2), 209-218. doi:10.1016/j.bbadis.2014.05.006

Ye, Y. H., Meyer, H. H., & Rapoport, T. A. (2001). The AAA ATPase Cdc48/p97 and its partners transport proteins from the ER into the cytosol. *Nature, 414*(6864), 652-656. doi:Doi 10.1038/414652a

Zhao, X., & Jantti, J. (2009). Functional characterization of the trans-membrane domain interactions of the Sec61 protein translocation complex beta-subunit. *BMC Cell Biol, 10*, 76. doi:10.1186/1471-2121-10-76

Zimmerberg, J., & Kozlov, M. M. (2006). How proteins produce cellular membrane curvature. *Nature Reviews Molecular Cell Biology, 7*(1), 9-19. doi:10.1038/nrm1784

Zinser, E., Paltauf, F., & Daum, G. (1993). Sterol composition of yeast organelle membranes and subcellular distribution of enzymes involved in sterol metabolism. *J Bacteriol, 175*(10), 2853-2858.

FIGURES

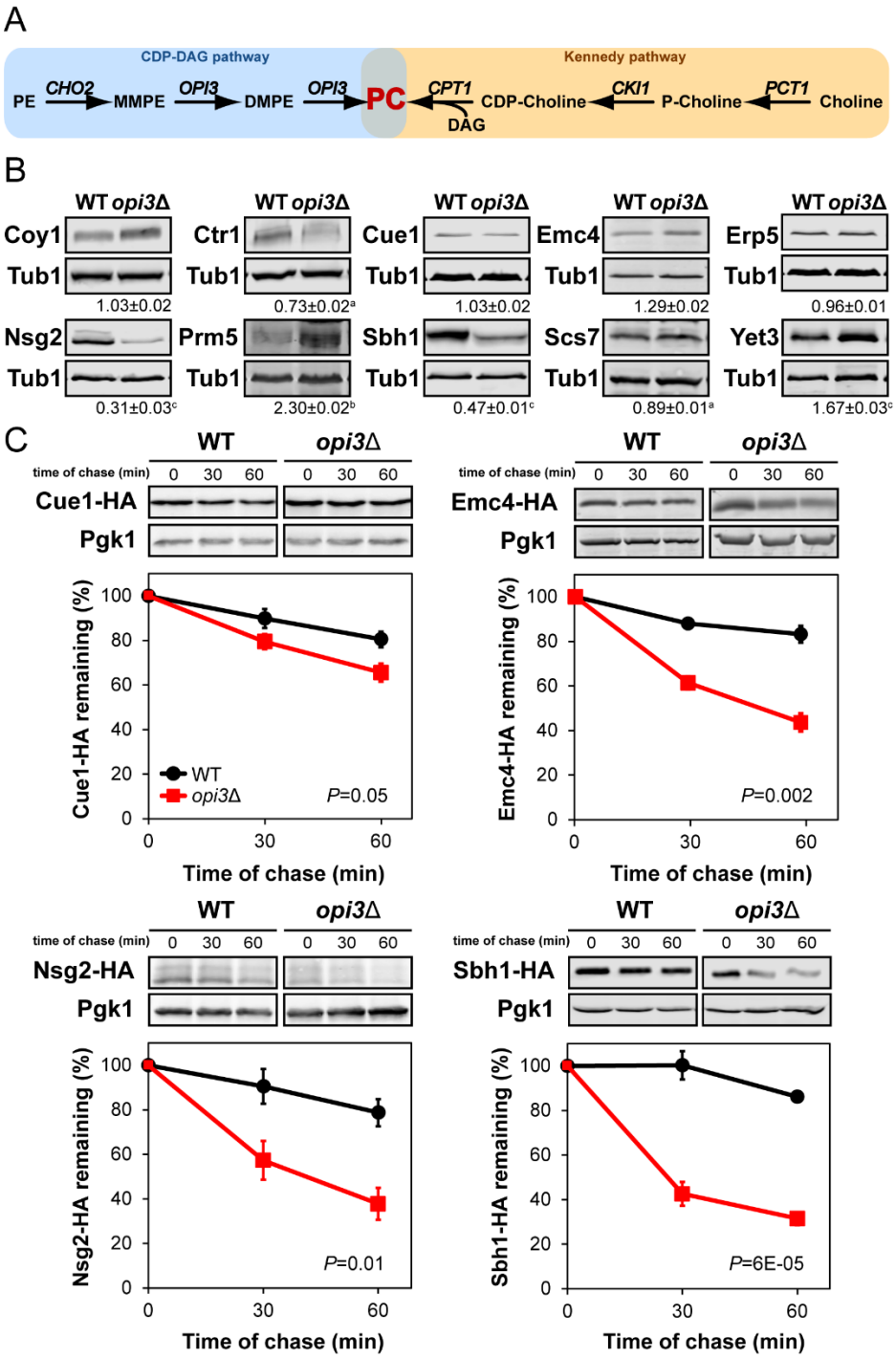

Figure 1. A subset of ER transmembrane proteins is pre-maturely degraded under lipid imbalance.
(A) Metabolic pathways for the synthesis of phosphatidylcholine in *S. cerevisiae*. PE, phosphatidylethanolamine; MMPE, N-monomethyl phosphatidylethanolamine; DMPE, N,N-dimethyl phosphatidylethanolamine; PC, phosphatidylcholine; DAG, diacylglycerol; P-choline, phosphate-choline. (B) Steady state level of transmembrane proteins. Equal cell numbers were harvested. Proteins were separated by SDS-PAGE and detected by immunoblotting with antibodies against the HA tag and Tub1 as loading control. $^{a}P < 0.05$, $^{b}P < 0.01$, $^{c}P < 0.005$, Student's t test. (C) Degradation of HA-tagged proteins was analysed after blocking protein translation with cycloheximide. Proteins were separated by SDS-PAGE and detected by immunoblotting with antibodies against the HA tag and Pgk1 as loading control.

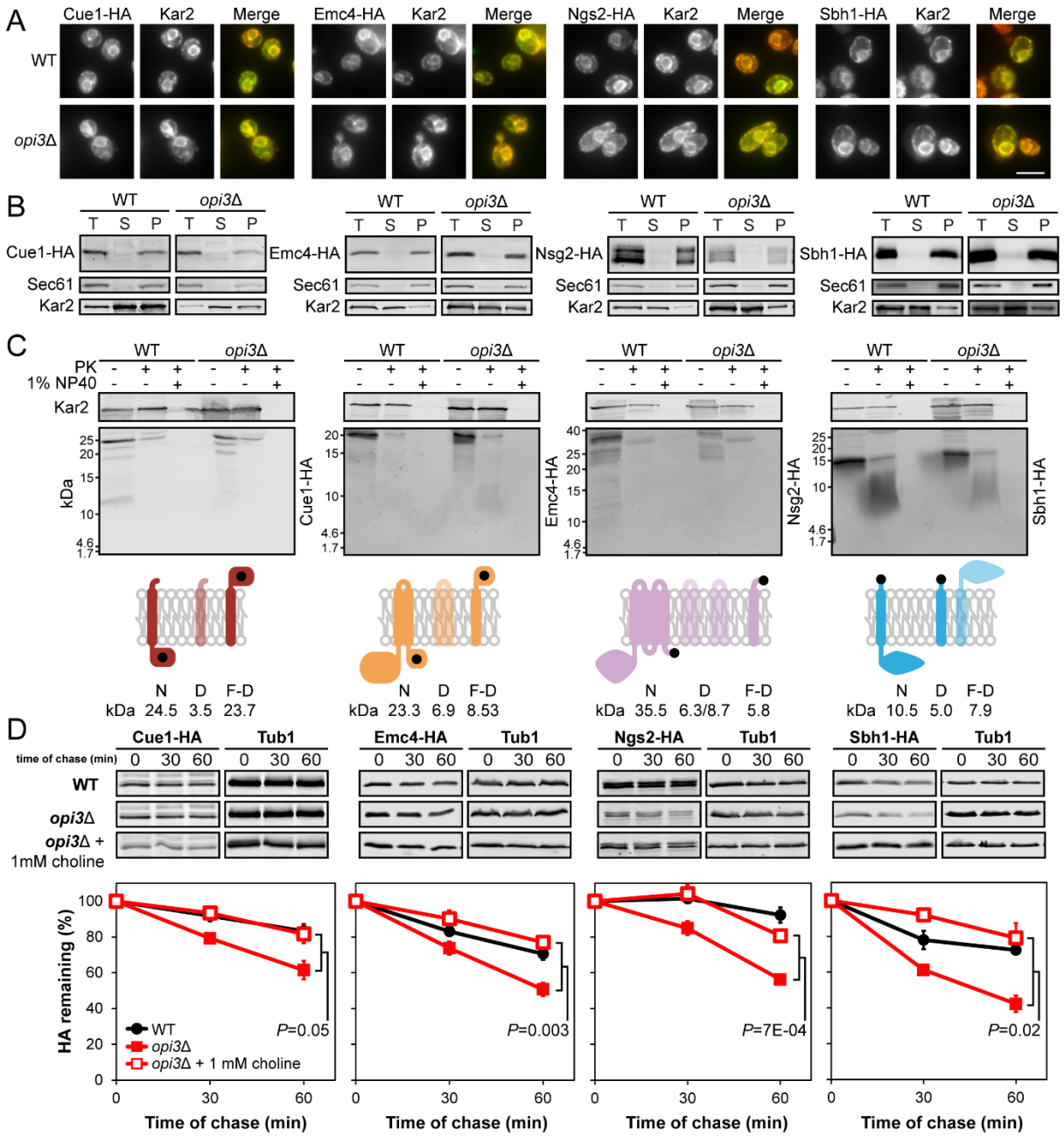

Figure 2. Transmembrane proteins are destabilised by the decrease in phosphatidylcholine synthesis.
(A) Protein candidates were detected using antibodies against HA tag and Kar2 antibody as ER marker. Scale bar, 5 µm. (B) Membranes prepared from wild type and *opi3*Δ expressing HA tagged proteins were treated with 0.1 M sodium carbonate, pH 11, for 30 min on ice. A portion was reserved as total (T), and the remaining was subjected to centrifugation at 100,000 x *g*. Supernatant (S) and membrane pellet (P) fractions were collected and analysed by immunoblotting. Proteins were detected using anti-HA antibody. Kar2 and Sec61 serve as soluble and integral membrane protein controls, respectively. (C) Membranes prepared from WT and *opi3*Δ cells expressing HA tagged proteins were treated with 1 mg/ml proteinase K, for 30 min at 37°C, with or without 1% NP40. HA-tagged were precipitated with 10% TCA, separated by SDS-PAGE and detected by immunoblotting with HA antibody. Expected proteins molecular weight are shown below for non-digested (N), digested (D), and flipped and digested (F-D). HA tag is shown as black dot. Fragments missing HA tag are not detectable and are illustrated with transparency. ER lumen and cytosol are at the top and bottom of the membrane, respectively. (D) Cell were grown in the absence or presence of 1 mM choline before addition of cycloheximide. Time point were taken as indicated. Proteins were separated by SDS-PAGE and detected by immunoblotting with antibodies against HA tag and Tub1 as loading control.

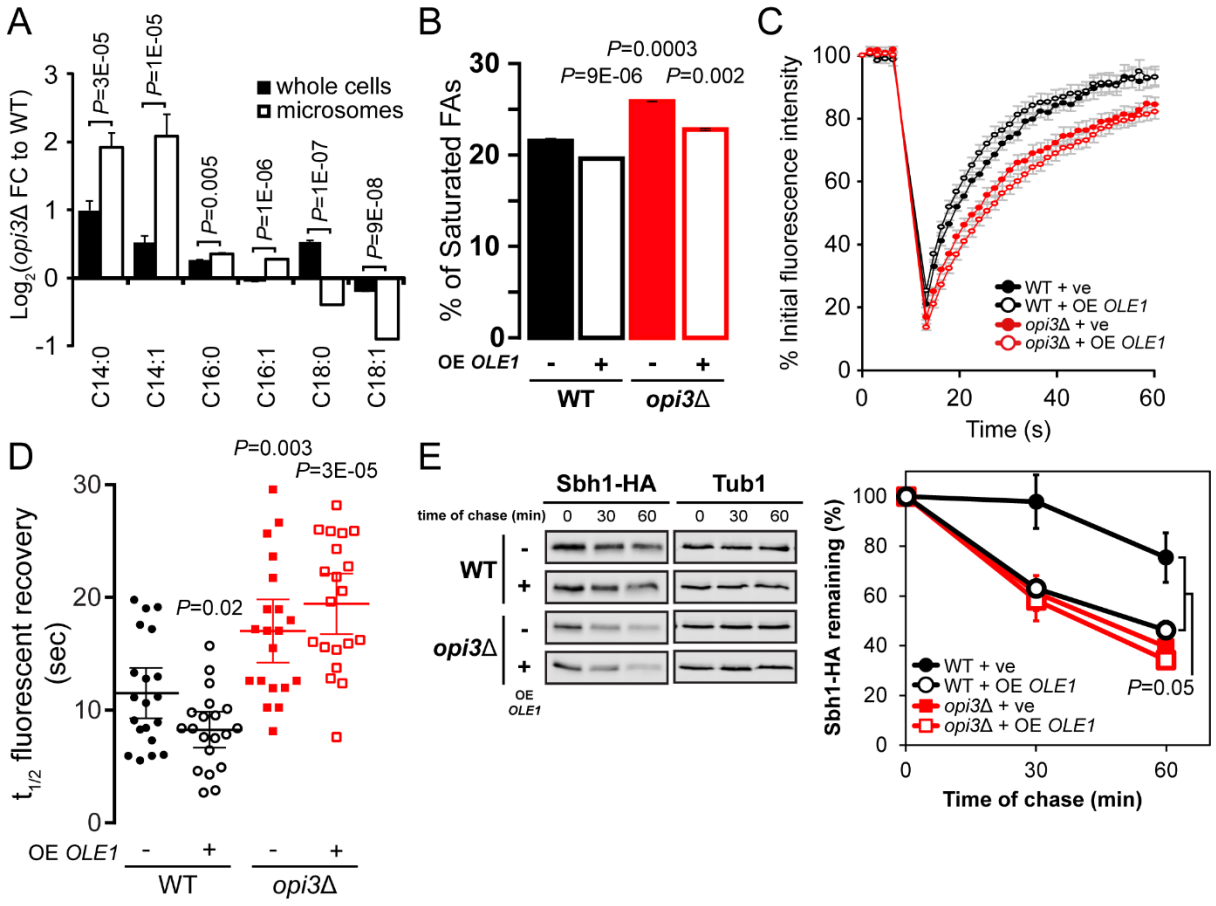

Figure 3. Sbh1 is destabilised from increased membrane fluidity of the ER membrane.
(A) Fold changed (FC) of FAs in *opi3*Δ is compared to WT. Total FA in whole cells and microsomes of WT and *opi3*Δ were quantified by gas chromatography after FAME derivatisation. (B) Percentage of saturated fatty acids to total FAs in *opi3*Δ, WT and *opi3*Δ both overexpressing (OE) *OLE1* under the control of *PRC1* promoter is compared to WT. FAs were detected as in B. Student's t test compared to WT. (C,D) Fluorescent recovery of Sec63-GFP in *opi3*Δ, WT and *opi3*Δ both OE *OLE1* is compared to WT after photobleaching. A region of the cortical ER of live cells were photobleached and recovery points of 1.5 s interval were taken. Fluorescence recovery after photobleaching (FRAP) is shown for the first 60 seconds from the average of 20 cells (C). The time taken for the recovery of half the maximum fluorescent ($t_{½}$) was calculated and plotted (D). Student's t test compared to WT. (E) The degradation of Sbh1-HA in WT and *opi3*Δ cells was analysed in the absence (control vector) or presence of OE *OLE1* after blocking translation with cycloheximide. Proteins were separated by SDS-PAGE and detected by immunoblotting with antibodies against HA tag and Tub1 as loading control.

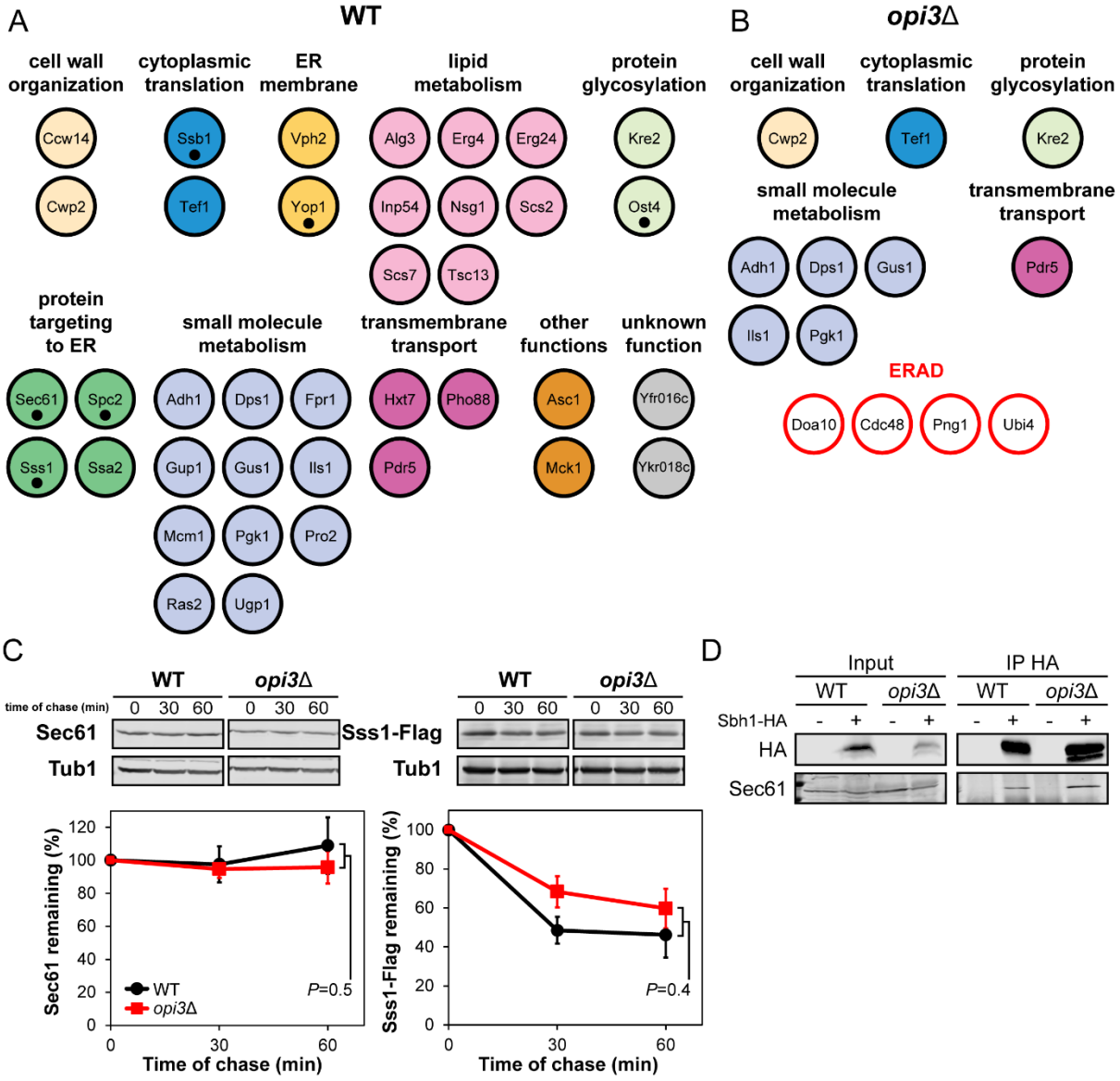

Figure 4. Sbh1 dissociates from Sec61 complex under lipid imbalance.
(A,B) Proteins identified as interacting partners of N-tagged (TF-Cub-Sbh1) by the MYTH method in WT (A) and *opi3*Δ (B) cells. ERAD factors were only detected in *opi3*Δ and are denoted in red. Previously reported interactors of Sbh1 are indicated with black dots. (C) The degradation of Sec61 or Sss1-Flag was analysed in WT and *opi3*Δ cells after blocking translation with cycloheximide. Proteins were separated by SDS-PAGE and detected by immunoblotting with antibodies against Sec61 or Flag tag and Tub1 as loading control. (D) Immunoprecipitation of Sbh1-HA with protein G beads were analysed in WT and *opi3*Δ cells after proteins were cross-linked with DTBP. Elution and input samples were resolved by SDS-PAGE, transferred to nitrocellulose membrane, and analysed by immunoblot with antibodies against Sec61 and the HA tag after the release of HA bound Sbh1 with HA peptide.

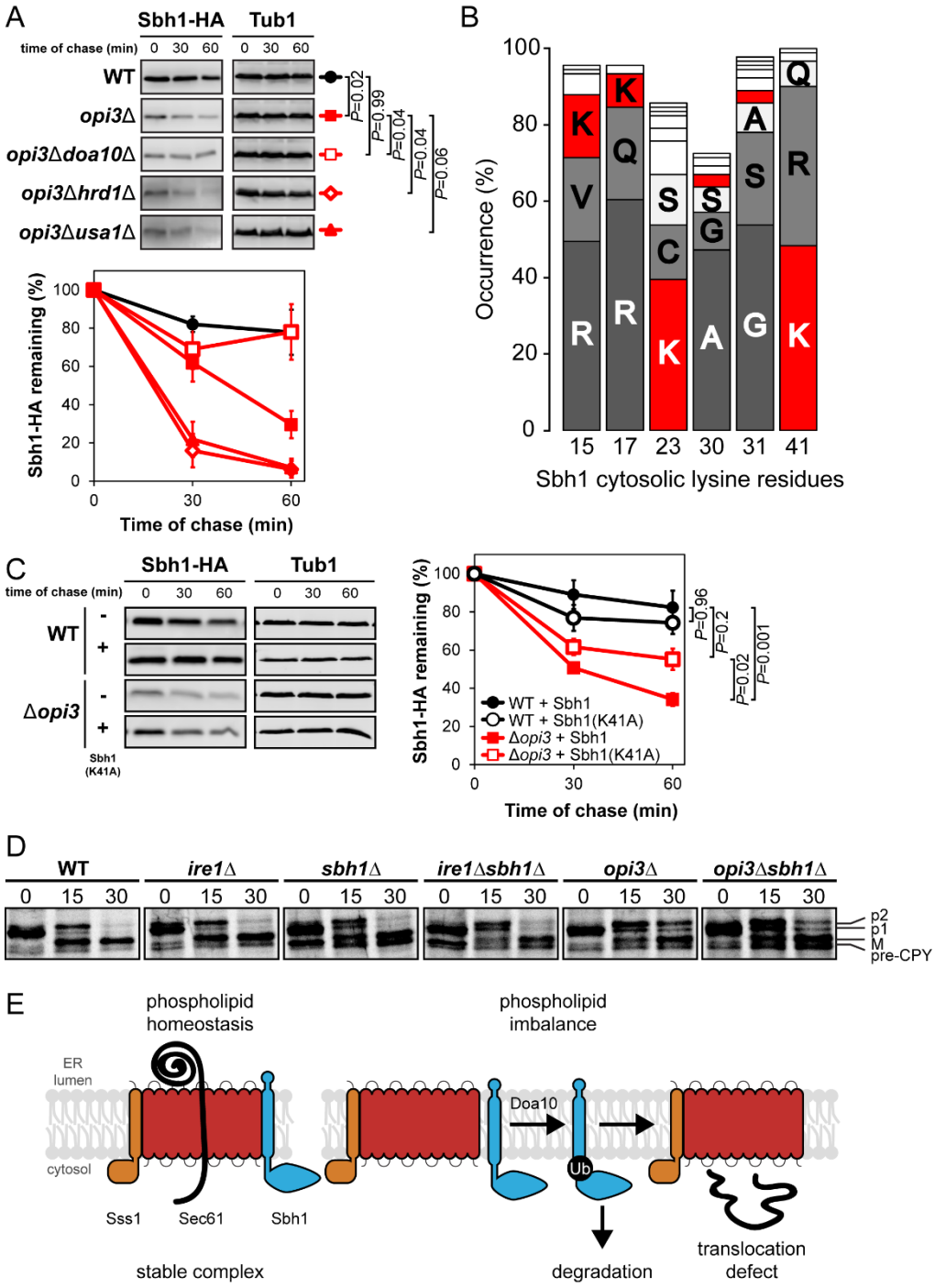

Figure 5. Sbh1 is recognised and degraded by ERAD from its cytoplasmic domain under lipid imbalance.
(A) The degradation of Sbh1-HA was analysed in WT, *opi3*Δ, *opi3*Δ*doa10*Δ, *opi3*Δ*hrd1*Δ, and *opi3*Δ*usa1*Δ cells after blocking translation with cycloheximide. Proteins were separated by SDS-PAGE and detected by immunoblotting with antibodies against the HA tag and Tub1 as loading control. (B) Sbh1 sequences from 90 different eukaryotes were aligned. The top three amino acids corresponding to the cytosolic lysine residues (shown in red) of *S. cerevisiae* Sbh1 are shown. (C) The degradation of Sbh1-HA or Sbh1(K41A)-HA was analysed in WT and *opi3*Δ cells as in A. (D) Cells were grown to early log phase in selective synthetic complete media before being pulse-labelled with L-[^{35}S]-methionine/cysteine for 5 min followed by a chase at the indicated times. Immunoprecipitated proteins using anti-CPY were resolved by SDS-PAGE and visualised by phosphoimager analysis. (E) Under LP, Sbh1 dissociates from the Sec61 complex and is recognised and ubiquitylated by the Doa10 complex leading to Sbh1 degradation from the proteasome. This results in translocation defect of Sbh1-depleted Sec61 complexes.

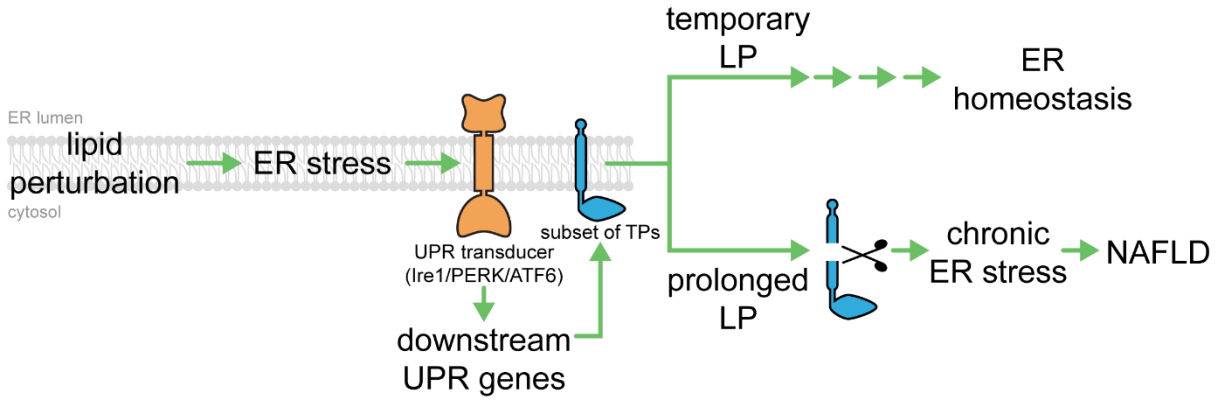

Figure 6. Premature degradation of TPs leads to chronic ER stress and development of NAFLD. Normally, ER homeostasis can be reached from lipid perturbation through the regulation of downstream UPR target genes. UPR transactivator (yellow protein representing Ire1, PERK, or ATF6) senses ER stress from the accumulation of misfolded proteins and/or lipid perturbation. However, if LP is prolonged, ER homeostasis might not be reached due to the premature degradation of a subset of misfolded proteins (blue protein) leading to chronic ER stress, cell death, and eventually the development of NAFLD.

SUPPLEMENTAL INFORMATION

Lipid Perturbation compromises the activation of the unfolded protein response

Benjamin S.H. Ng, Peter Jr. Shyu, Ruijie Chaw, Seah Yi Ling, Guillaume Thibault

INVENTORY OF SUPPLEMENTAL INFORMATION

1. **Figure S1**, Refers to **Figure 1D**. **Sbh1 is highly conserved from yeast to humans**
2. **Figure S2**, Refers to **Figure 2**. **Strong activation of the UPR does not destabilise Sbh1**
3. **Figure S3**, Refers to **Figure 3B**. **Lack of *OPI3* leads to broad remodelling of fatty acids**
4. **Figure S4**, Refers to **Figure 3D-E**. **Time-lapse images of Sec63-GFP by FRAP**
5. **Figure S5**, Refers to **Figure 4A-B**. **Validation of Sbh1 interacting partners**
6. **Figure S6**, Refers to **Figure 5A**. **Sbh1 is degraded by the ERAD and not the vacuolar pathways**
7. **Figure S7**, Refers to **Figure 5D**. **The lack of *SBH1* does not lead to ER stress**
8. **Table S1**, Refers to **Figures 1A-B**. **List of genes upregulated transcriptionally but having lower protein abundance under LP.** Excel Spreadsheet
9. **Table S2**. **List of *Saccharomyces cerevisiae* strains used in the study**
10. **Table S3**. **List of plasmids used in the study**
11. **Table S4**. **List of primers used in the study**

SUPPLEMENTAL INFORMATION

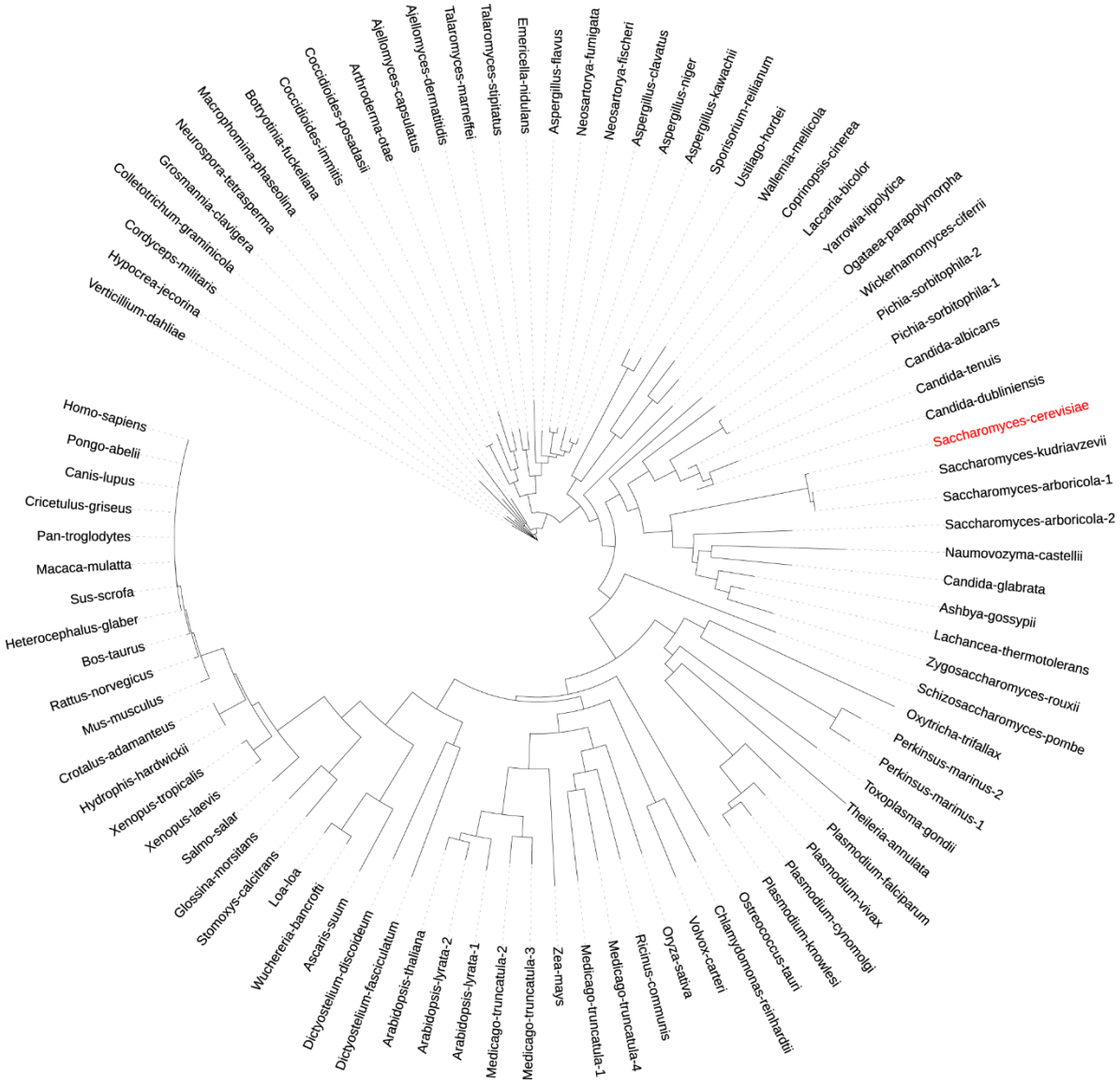

Figure S1. Sbh1 is highly conserved among eukaryotes.
Sbh1 protein sequence was blasted with NCBI Protein BLAST and 90 homologs were identified. The sequences were aligned with Cluster Omega. The phylogenetic tree was constructed with iTOL v3.

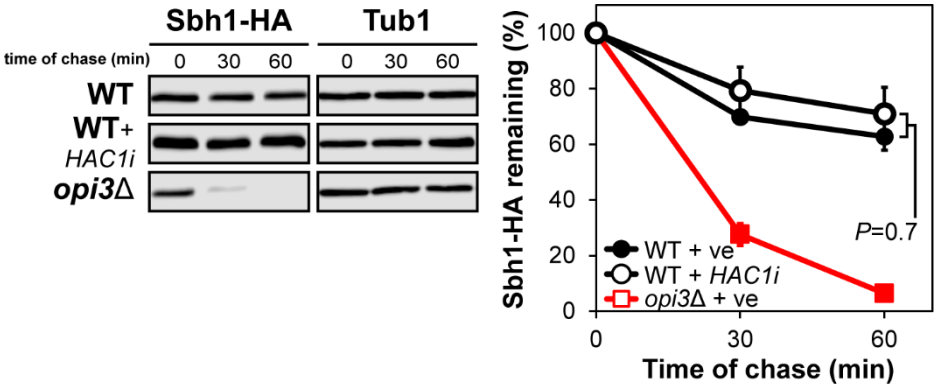

Figure 2. **Strong activation of the UPR does not destabilise Sbh1.**
The degradation of Sbh1-HA was analysed in WT and *opi3*Δ cells containing control vector (ve) or *HAC1*^{i}-bearing plasmid after blocking translation with cycloheximide. Proteins were separated by SDS-PAGE and detected by immunoblotting with antibodies against HA tag and Tub1 as loading control.

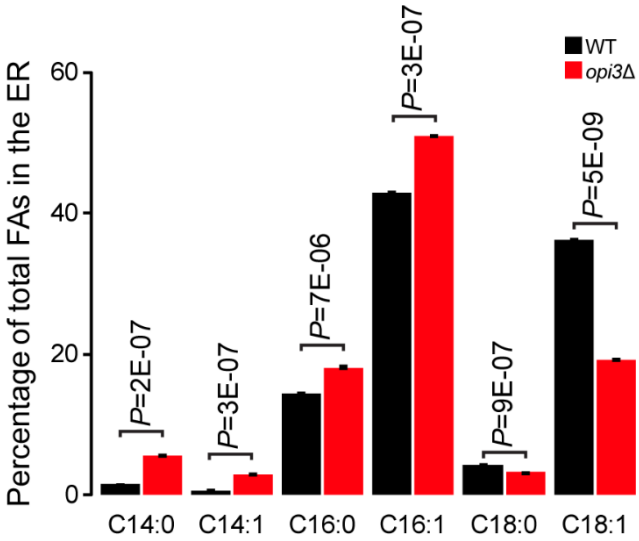

Figure S3. Lack of *OPI3* leads to broad remodelling of fatty acids.
Percentage of fatty acid chain lengths to total fatty acids in *opi3*Δ is compared to WT. Total fatty acid content in microsomes of WT and *opi3*Δ were quantified by gas chromatography after FAME derivatisation.

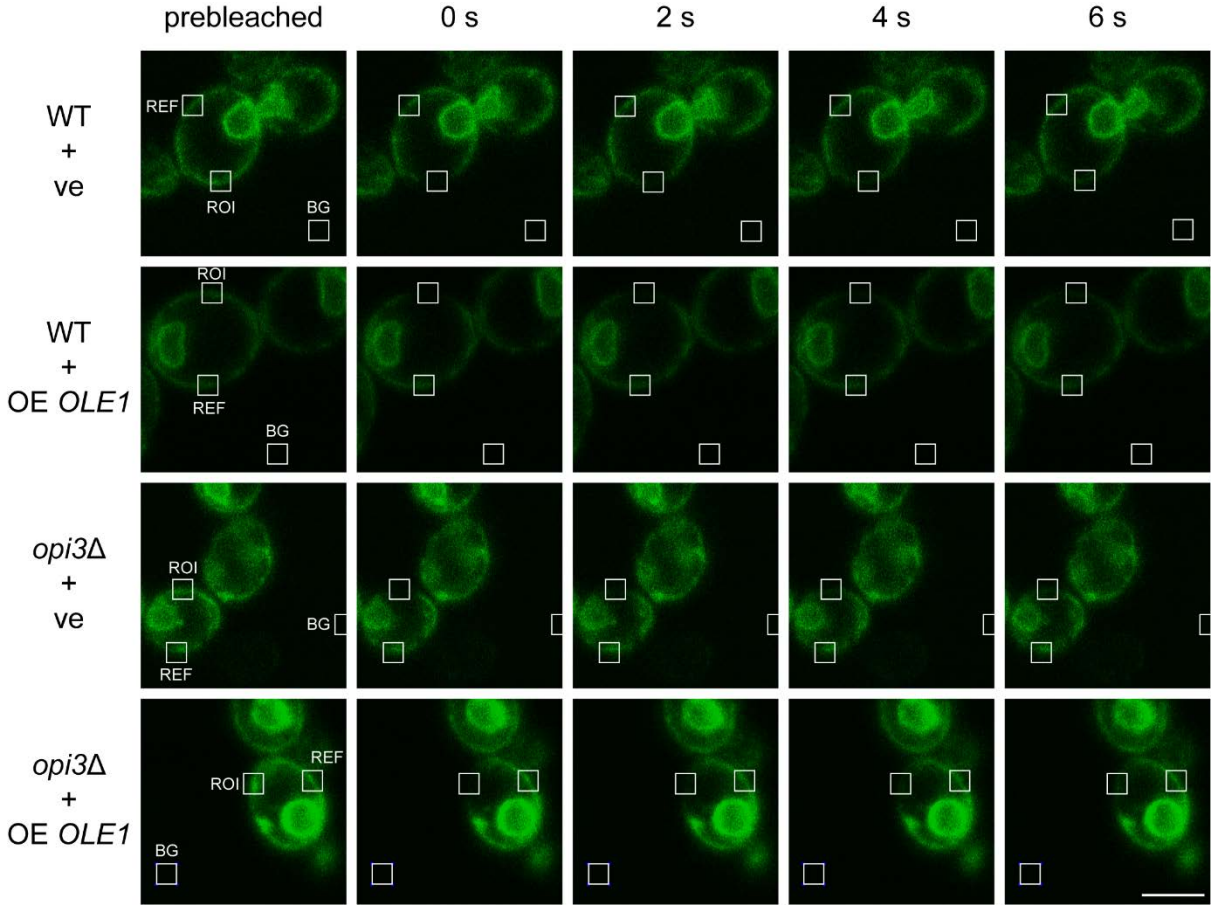

Figure S4. Time-lapse images of Sec63-GFP by FRAP.
Time-lapse images of Sec63-GFP by FRAP. Images were taken before (prebleanched) and at time indicated following photobleaching. Fluorescence intensity was monitored from the white boxes ROI (region of interest), REF (reference), and BG (background). Scale bar, 5 µm.

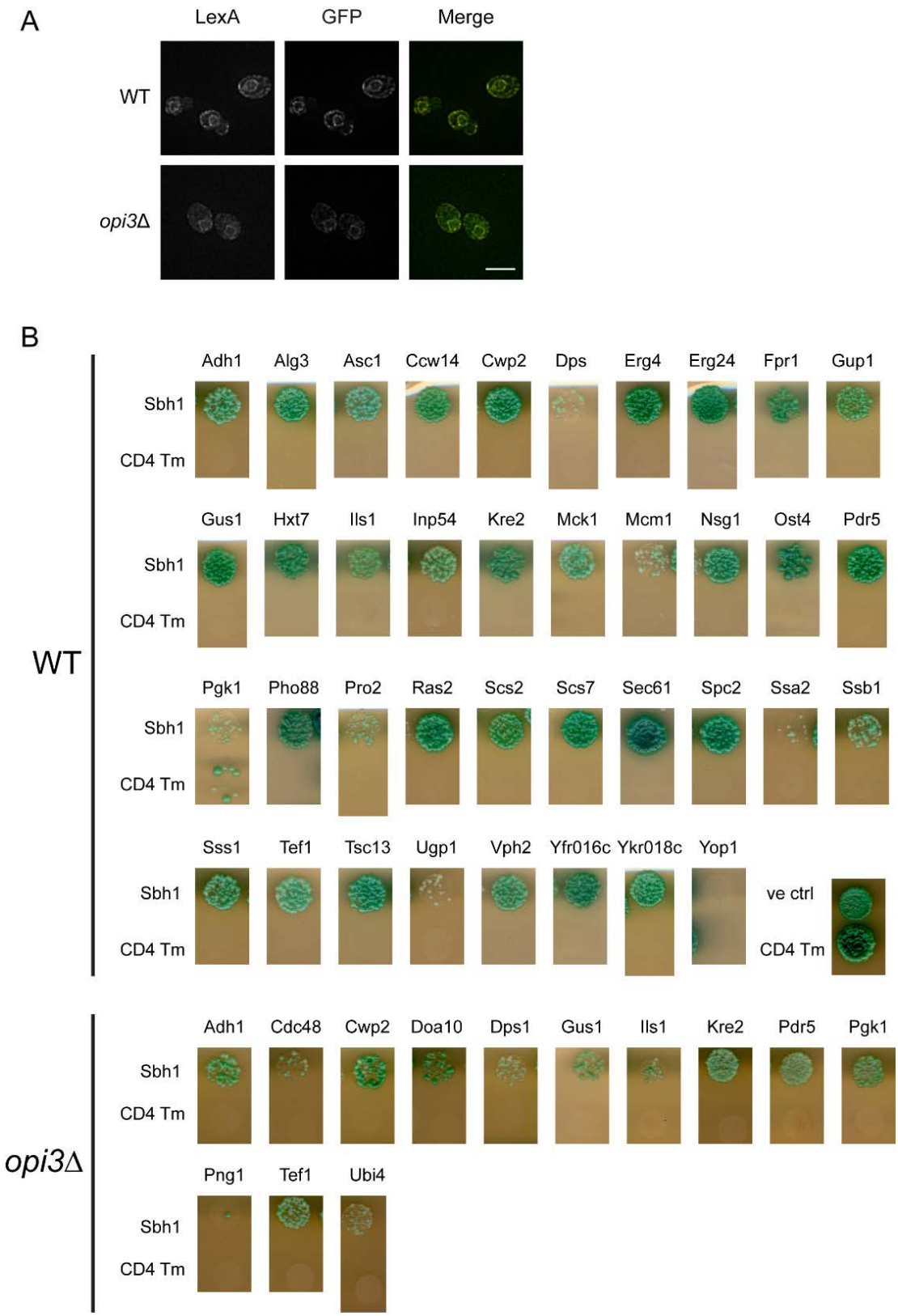

Figure S5. Validation of Sbh1 interacting partners.
(A) N-tagged (TF-Cub-Sbh1) remains localised to the ER membrane in both WT and *opi3*Δ. Protein candidates were detected using antibodies against LexA and eroGFP as ER marker. Scale bar, 5 µm. (B) Interacting proteins of N-tagged (TF-Cub-Sbh1) were retransformed with the original bait strain, together with a negative control using the single-pass transmembrane domain of human T-cell surface glycoprotein CD4 tagged to Cub-LexA-VP16 MYTH. Positive control of pOST1-NubI bait was used (ve ctrl). Tm, tunicamycin.

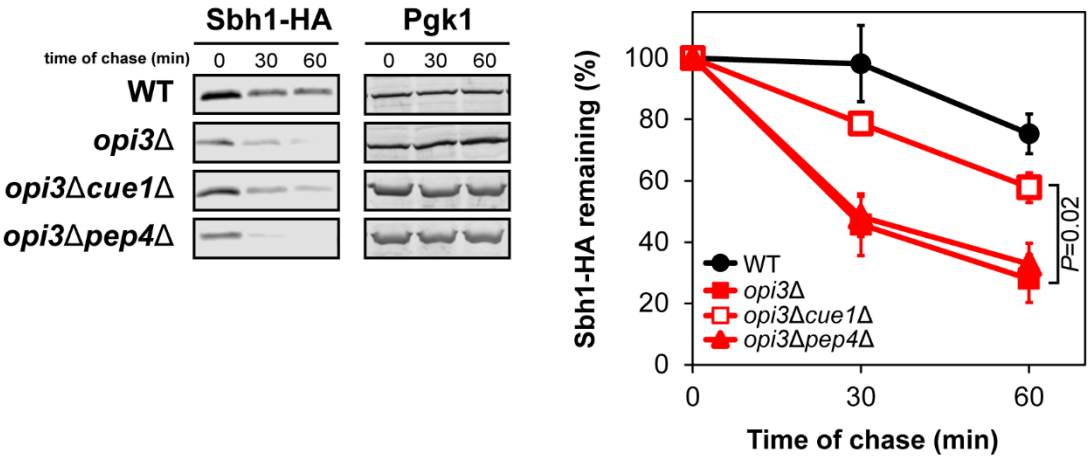

Figure S6. Sbh1 is degraded by the ERAD and not the vacuolar pathways.
The degradation of Sbh1-HA was analysed in WT, *opi3*Δ, *opi3*Δ*cue1*Δ, and *opi3*Δ*pep4*Δ cells after blocking translation with cycloheximide. Proteins were separated by SDS-PAGE and detected by immunoblotting with antibodies against the HA tag and PGK1 as loading control.

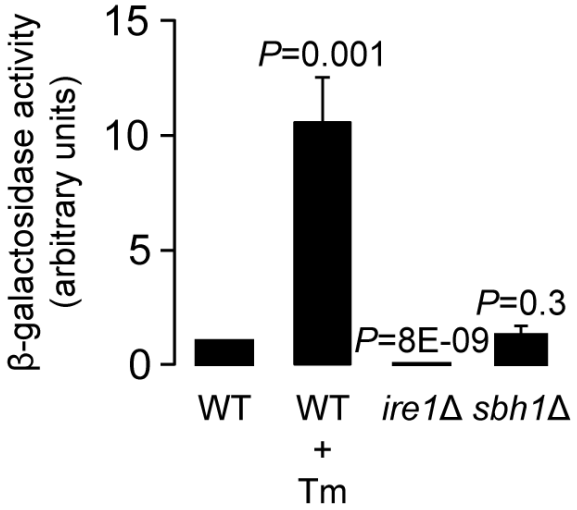

Figure S7. The lack of *SBH1* does not lead to ER stress.
Cells were grown to early log phase at 30˚C in selective synthetic complete media. UPR induction was measured using a *UPRE-LacZ* reporter assay. Tm, tunicamycin.

Table S2. **Strains used in the study**

Strains	Genotype	Source
W303a	*MATa, leu2-3,112, his3-11, trp1-1, ura3-1, can1-100, ade2-1*	(Cox, Shamu, & Walter, 1993)
GTY68	*MATa, opi3::KANMX,* W303 background	(Thibault et al., 2012)
YGT0315	*MAT*a, pGT0181, W303 background	This study
YGT0317	*MAT*a, *opi3::KANMX*, pGT0181, W303 background	This study
YGT0318	*MAT*a, pGT0182, W303 background	This study
YGT0320	*MAT*a, *opi3::KANMX*, pGT0182, W303 background	This study
YGT0321	*MAT*a, pGT0179, W303 background	This study
YGT0323	*MAT*a, *opi3::KANMX*, pGT0179, W303 background	This study
YGT0327	*MAT*a, pGT0185, W303 background	This study
YGT0329	*MAT*a, *opi3::KANMX*, pGT0185, W303 background	This study
YGT0330	*MAT*a, pGT0315, W303 background	This study
YGT0332	*MAT*a, *opi3::KANMX*, pGT0315, W303 background	This study
YGT0374	*MAT*a, pGT0183, W303 background	This study
YGT0375	*MAT*a, *opi3::KANMX*, pGT0183, W303 background	This study
YGT0432	*MAT*a, pJC835, W303 background	This study
YGT0540	*MAT*a, pGT0288, NMY51 background (*his3Δ200*, *trp-901*, *leu2-3*,*112*, *ade2*, *LYS::(lexAop)4-HIS3*, *ura3::(lexAop)8-LACZ*, *(lexAop)8-ADE2*, *GAL4*)	This study
YGT0541	MATa, *opi3::KANMX*, pGT0183, NMY51 background	This study
YGT0574	*MAT*a, *doa10::KANMX*, *opi3::KANMX*, pGT0183, W303 background	This study
YGT0575	*MAT*a, *hrd1::KANMX*, *opi3::KANMX*, pGT0183, W303 background	This study
YGT0576	*MAT*a, *usa11::KANMX*, *opi3::KANMX*, pGT0183, W303 background	This study
YGT0671	*MAT*a, pGT0352, W303 background	This study
YGT0672	*MAT*a, *opi3::KANMX*, pGT0352, W303 background	This study
YGT0673	*MAT*a, pGT0183, pRS313, W303 background	This study
YGT0674	*MAT*a, *opi3::KANMX*, pGT0183, pRS313, W303 background	This study
YGT0675	*MAT*a, pGT0183, pGT0349, W303 background	This study
YGT0676	*MAT*a, *opi3::KANMX*, pGT0183, pGT0349, W303 background	This study
YGT0690	*MAT*a, pGT0180 , W303 background	This study
YGT0691	*MAT*a, *opi3::KANMX*, pGT0180, W303 background	This study
YGT0721	*MAT*a, pGT0350, pGT0183, W303 background	This study
YGT0722	*MAT*a, *opi3::KANMX*, pGT0350, pGT0183, W303 background	This study
YGT0725	*MAT*a, pGT0350, pRS315, W303 background	This study
YGT0726	*MAT*a, *opi3::KANMX*, pGT0350, pRS315, W303 background	This study
YGT0769	*MAT*a, pGT0366, W303 background	This study
YGT0770	*MAT*a, *opi3::KANMX*, pGT0366, W303 background	This study
YGT0771	*MAT*a, pGT0368, W303 background	This study
YGT0772	*MAT*a, *opi3::KANMX*, pGT0368, W303 background	This study
YGT0773	*MAT*a, pGT0365, W303 background	This study
YGT0774	*MAT*a, *opi3::KANMX*, pGT0365, W303 background	This study
YGT0874	*MAT*a, pPS1622, pRS313, W303 background	This study
YGT0875	*MAT*a, *opi3::KANMX*, pPS1622, pRS313, W303 background	This study
YGT0876	*MAT*a, pGT0349, pPS1622, W303 background	This study
YGT0877	*MAT*a, *opi3::KANMX*, pGT0349, pPS1622, W303 background	This study

Table S3. Plasmids used in the study

Plasmid	Encoded protein	Promoter	Vector	Source
pJC31	β-galactosidase	*UPRC-CYC1*	pRS315	(Cox & Walter, 1996)
pPS1622	Sec63-sGFP	*SEC63*	pRS316	(Prinz et al., 2000)
pJC835	Hac1	*HAC1*	pRS313	(Spear & Ng, 2003)
pGT0284	IRE1-3X FLAG	*IRE1*	pRS426	(Kimata, Oikawa, Shimizu, Ishiwata-Kimata, & Kohno, 2004)
pPM28	eroGFP	*GAP*	pRS316	(Merksamer, Trusina, & Papa, 2008)
pGT0179	Nsg2-HA	*NSG2*	pRS315	This study
pGT0181	Cue1-HA	*CUE1*	pRS315	This study
pGT0183	Sbh1-HA	*SBH1*	pRS315	This study
pGT0185	Emc4-HA	*EMC4*	pRS315	This study
pGT0288	Cub-LexA-VP16-Sbh1	*CYC1*	pBT3-N	This study
pGT0349	Ole1-3XFlag	*PRC1*	pRS313	This study
pGT0352	Sbh1(K41A)-HA	*SBH1*	pRS315	This study
pGT0350	Sss1-3XFlag	*SSS1*	pRS313	This study

Table S4. **Oligonucleotide primers used in the study**

Primer	Sequence (5' to 3')
BN001	AGTATACATACGGATCCATGCCAACTTCTGGAACTAC
BN002	GTAGTCCGCATGCCCTTAAAAGAACTTACCAGTTTCG
BN013	AGTATACATACGGATCCATGGCTAGAGCTAGTGAAAAAG
BN014	GTAGTCCGCATGCCCTTAAACAATAACGTATCTGATTG
BN015	GGGCATGCGGACTACAAA
BN016	GGATCCGTATGTATACTTTAAGTTGAG
BN017	AGCTTTCCACCTGGGTTTGAGC
BN018	CGCCACCAGCAGCGTTATTATC
BN019	ACTGCCCTCATGCTACTCTCTG
BN020	ACCCAACACTGGTTTGAATGCAC
BN021	TCTGATGAGGCTACGGGACTAAG
BN022	AACCGACCGCTAGAAACAACAC
BN023	GGAGAACCGGATCCAAAGAAGAGC
BN024	AAGCTGCGGTTTAGTCAGAGAGC
BN025	TGGATTCTGAGGTTGCTGCTTTGG
BN026	ACCTTGGTGTCTTGGTCTACCG
BN027	ATGAGGGCCATTACGGCCATGTCAAGCCCAACTCCTCC
BN028	CTCATGGCCGAGGCGGCCTTAAAATAACTTACCGGCAACTTTAGAATAACATG
BN029	CTCATGCTGCAGATGGAGGATTCGAGATTGCTTATCACTTTG
BN030	CTCATGCCATGGGAGTCAGCAAACTTTGCAAATCTTTATCAC
BN031	AACGTCGCGGCCGCAGCAAATGATTCCTCGACTGAATATAAAGG
BN032	CCATGGCGCGCTAATCGGAAAACCATTGTAATCCATTATTATAATGAGCA
BN033	CTCATGCTGCAGATGGCCAATAGAGGAGAACCGG
BN034	CTCATGCCATGGGATGAGAATATAGATATCTTCCTAGTTTTCCAAACA
BN035	CTCATGCTGCAGATGTCAAGCCCAACTCCTCC
BN036	CTCATGCCATGGGAAATAACTTACCGGCAACTTTAGAAATAACATG
BN037	AATTCGATTTTGGCGATTTATTCTGAT
BN038	ATTGCTGTTCGTGTTTTTCTTTGGAGC

SUPPLEMENTAL REFERENCES

Cox, J. S., Shamu, C. E., & Walter, P. (1993). Transcriptional Induction of Genes Encoding Endoplasmic-Reticulum Resident Proteins Requires a Transmembrane Protein-Kinase. *Cell, 73*(6), 1197-1206. doi:Doi 10.1016/0092-8674(93)90648-A

Cox, J. S., & Walter, P. (1996). A novel mechanism for regulating activity of a transcription factor that controls the unfolded protein response. *Cell, 87*(3), 391-404.

Kimata, Y., Oikawa, D., Shimizu, Y., Ishiwata-Kimata, Y., & Kohno, K. (2004). A role for BiP as an adjustor for the endoplasmic reticulum stress-sensing protein Ire1. *J Cell Biol, 167*(3), 445-456. doi:10.1083/jcb.200405153

Merksamer, P. I., Trusina, A., & Papa, F. R. (2008). Real-time redox measurements during endoplasmic reticulum stress reveal interlinked protein folding functions. *Cell, 135*(5), 933-947. doi:10.1016/j.cell.2008.10.011

Prinz, W. A., Grzyb, L., Veenhuis, M., Kahana, J. A., Silver, P. A., & Rapoport, T. A. (2000). Mutants affecting the structure of the cortical endoplasmic reticulum in Saccharomyces cerevisiae. *J Cell Biol, 150*(3), 461-474.

Spear, E. D., & Ng, D. T. (2003). Stress tolerance of misfolded carboxypeptidase Y requires maintenance of protein trafficking and degradative pathways. *Mol Biol Cell, 14*(7), 2756-2767. doi:10.1091/mbc.E02-11-0717

Thibault, G., Shui, G., Kim, W., McAlister, G. C., Ismail, N., Gygi, S. P., . . . Ng, D. T. (2012). The membrane stress response buffers lethal effects of lipid disequilibrium by reprogramming the protein homeostasis network. *Mol Cell, 48*(1), 16-27. doi:10.1016/j.molcel.2012.08.016